frontiers in Earth Science

ORIGINAL RESEARCH
published: 04 January 2019
doi: 10.3389/feart.2018.00236

Dynamics of Manganese and Cerium Enrichments in Arctic Ocean Sediments: A Case Study From the Alpha Ridge

Liming Ye[1,2], Christian März[3], Leonid Polyak[2], Xiaoguo Yu[1] and Weiyan Zhang[1]*

[1] Key Laboratory of Submarine Geosciences, Second Institute of Oceanography, State Oceanic Administration, Hangzhou, China, [2] Byrd Polar and Climate Research Center, The Ohio State University, Columbus, OH, United States, [3] School of Earth and Environment, University of Leeds, Leeds, United Kingdom

Manganese (Mn) and cerium (Ce) are known as reactive metals sensitive to marine redox conditions, and can therefore serve as useful proxies for paleoceanographic environments. Quaternary sedimentary records in the Arctic Ocean show a consistent cyclicity of Mn enrichments, but Mn sources, transportation and deposition patterns, and relationship to paleoclimatic conditions are not well understood. Sediment core ARC3-B85D from the Alpha Ridge with the estimated stratigraphy covering ~350 kyr is used to investigate a coupled distribution of Mn and Ce in Quaternary Arctic Ocean sediments. By analyzing Mn and Ce distribution patterns in the core and surface sediments from the western Arctic Ocean and adjacent shelves, we investigate the conditions and dynamics of concurrent metal enrichments. Stratigraphic Ce and Mn patterns follow inferred glacial-interglacial cycles, with enrichments generally occurring during interglacial-type conditions with high sea levels. However, the relationships involved are not straightforward as highest Mn and Ce enrichments seem to occur closer to the end of interglacial/major interstadial periods, when sea levels were lowering from their highest positions. We conclude that the enrichment patterns are primarily defined by sediment dynamics controlling resuspension and transportation of reactive metals and their deposition in the central Arctic Ocean after diagenetic preconditioning on the shelves. We further infer that major transportation agents are sea-level affected cross-shelf and mid-depth ocean currents rather than sea ice as has been proposed earlier. Comprehending this coupled geochemical and sedimentary system is important for improving the chronostratigraphic framework for Quaternary deposits in the Arctic Ocean.

Keywords: Arctic Ocean, reactive metals, sea level, paleoceanography, sedimentary stratigraphy, Quaternary

OPEN ACCESS

Edited by:
Thomas Mark Cronin, United States Geological Survey, United States

Reviewed by:
Dennis A. Darby, Old Dominion University, United States
Ludvig Löwemark, National Taiwan University, Taiwan

****Correspondence:***
Liming Ye
lmye@sio.org.cn

Specialty section:
This article was submitted to Quaternary Science, Geomorphology and Paleoenvironment, a section of the journal Frontiers in Earth Science

Received: *26 June 2018*
Accepted: *04 December 2018*
Published: *04 January 2019*

Citation:
Ye L, März C, Polyak L, Yu X and Zhang W (2019) Dynamics of Manganese and Cerium Enrichments in Arctic Ocean Sediments: A Case Study From the Alpha Ridge. Front. Earth Sci. 6:236. doi: 10.3389/feart.2018.00236

INTRODUCTION

The fundamental challenge in Arctic paleoceanography is a lack of reliable chronostratigraphic age constraints, and thus the ability to compare Arctic Ocean sedimentary records to those from other oceans. The most widely accepted approach to constructing age models for Arctic Ocean Quaternary paleo-records is based on the apparently cyclic, glacial-interglacial changes in

depositional environments reflected in sediment stratigraphy (e.g., Jakobsson et al., 2000; Polyak et al., 2004; Spielhagen et al., 2004; O'Regan et al., 2008; Stein et al., 2010). In this approach, brown, manganese (Mn) enriched layers in Arctic sediment cores were suggested to represent interglacials and major interstadials, important as potential paleo-analogs for comprehending the modern climate change.

Mn (oxyhydr)oxides, which are characteristic for brown layers, provide sorption sites for other metals, resulting in enrichments of reactive Fe, Co, Mo, Ni, and Rare Earth Elements (REEs), like Ce, which are closely related to Mn and should thus be equally sensitive to redox conditions (Moffett, 1990; Haley et al., 2004; März et al., 2011a). While the use of Mn as a proxy for interglacial conditions may be complicated by early diagenesis, application of this approach provides climatically meaningful age constraints for Quaternary sediments on orbital timescales (Jakobsson et al., 2000; Adler et al., 2009; Schreck et al., 2018; Wang et al., 2018). Insights into sedimentary Mn sources, geochemical nature, and deposition aid understanding the mechanisms of brown layer formation and their environmental meaning (März et al., 2011a; Macdonald and Gobeil, 2012; Löwemark et al., 2014; Sundby et al., 2015). Approaches for constraining the diagenetic effects on Mn remobilization have also been suggested (März et al., 2011a; Meinhardt et al., 2016). Despite these advances, we are still vague on the sources, transportation, and deposition of Mn and related metals in the Arctic Ocean. In this paper we analyze paired Mn and Ce records in a sediment core from the Alpha Ridge, as well as surface sediments from the western Arctic Ocean, focusing on Mn and Ce sources, sedimentary sinks, and relationship to paleoclimatic conditions. We offer an explanation for the observed metal distribution that is based not only on the sources but also on differential transportation modes, leading to new insights into the spatial and temporal dynamics of Mn enrichment in Arctic Ocean sediments.

BACKGROUND

Metal Enrichment in Arctic Sediments

A number of transition metals recorded in Arctic Ocean sediment cores, such as Cu, Ni, Co, and Mo, share the same trends as Mn over glacial-interglacial cycles, since they are scavenged by the Fe–Mn (oxyhydr)oxides that precipitate from the water column and pore waters, and become enriched at the seafloor during interglacial-type conditions (März et al., 2011a; Meinhardt et al., 2014). Cerium (Ce), a Rare Earth Element (REE), often shows concurrent variations with Mn in ocean waters and sediments and is considered to have a redox behavior similar to Mn (Glasby, 1973; Elderfield et al., 1981; Bau and Koschinsky, 2009). However, analyses of the REE patterns in marine pore waters indicate that Ce may precipitate from solution in the form of Ce oxides independently from Mn (Moffett, 1990; Haley et al., 2004). *In situ* observation further demonstrate that trivalent light REE are preferentially absorbed onto Mn (oxyhydr)oxides in ocean surface waters but are mostly desorbed again in the deep ocean (Tachikawa et al., 1997). Only trivalent Ce that gets oxidized to tetravalent Ce in the sinking process is finally buried, leading to sediments with a positive Ce anomaly (Ce/Ce*, defined as the enrichment of Ce relative to its neighboring REEs La and Pr) (Tachikawa et al., 1997; Haley et al., 2014). Similar to Mn, in marine sediments Ce is expected to undergo early diagenetic remobilization once pore waters become oxygen-depleted as a result of organic matter degradation, which should lead to positive dissolved Ce/Ce* values. However, only few records of positive Ce anomalies have been reported from marine sedimentary pore waters within strongly reducing environments (Haley et al., 2004; Bau et al., 2014; Abbott et al., 2015), implying a simultaneous diffusion of dissolved Ce out of sediments, and/or its fast re-absorption/re-precipitation once pore water conditions are oxic again.

Based on previous studies, there are several geochemical properties that may cause Ce to behave differently from Mn. Unlike Mn, dissolved Ce occurs in seawater predominantly in strong carbonate complexes, which lower the activity of the free metal ion (Moffett, 1990; Johannesson et al., 2006). Further, Ce^{3+} has slower oxidation rates than Mn^{2+}, enabling dissolved Ce to cross the oxygenated sediment-water boundary more easily (De Baar et al., 1983; Soyol-Erdene and Huh, 2013). In addition, Ce oxides tend to be reduced under less strongly reducing conditions than Mn (oxyhydr)oxides, followed by Fe (oxyhydr)oxide reduction, when dissolved oxygen reaches a threshold of estimated < 10 μmol/L (Elderfield and Sholkovitz, 1987; Haley et al., 2004).

The sedimentary enrichments of Mn in the Arctic Ocean have been discussed in a number of publications from various perspectives (e.g., Jakobsson et al., 2000; Katsev et al., 2006; Löwemark et al., 2014), with much fewer studies addressing Ce records as well (Sangiorgi et al., 2008; März et al., 2011b). The stratigraphically long ACEX record from the Lomonosov Ridge in the central Arctic Ocean shows a pronounced positive Ce anomaly in the lower Miocene sediments interpreted to indicate the initiation of the deep water exchange with the Atlantic. However, no concurrent Mn enrichment was found, implying differences in the behavior of the two metals under variable redox conditions following the initial oxygenation of the Arctic Ocean (Sangiorgi et al., 2008; März et al., 2011b). No combined Ce–Mn records have been analyzed in more recent deposits characterized by strong glacial-interglacial cyclicity accentuated in sedimentary records by Mn enrichment in interglacial intervals. Based on estimates of the Arctic Ocean Mn budget and the exchange rates between the Arctic shelves and deep basins, sedimentary Mn variability has been explained by a combination of sea level changes and diagenetically induced sources for metal enrichment on the Arctic margins (Macdonald and Gobeil, 2012). Combined records of Ce and Mn, expected to have a somewhat different response to suboxic diagenetic conditions, have a potential to provide new insights into the drivers and mechanisms of Mn transport and deposition in the Arctic Ocean.

Sediment Transport and Deposition

Besides geochemical environments controlling initial oxidation and precipitation of reactive metals in the Arctic Ocean, sediment dynamics are also important for understanding transportation

and depositional processes leading to Mn enrichments in seafloor sediments. Unlike other oceans, sedimentation in the Arctic Ocean is largely defined by sea-ice and/or icebergs transporting terrigenous sediments from continental margins to the ocean interior, where transportation pathways are primarily determined by the surface circulation. At present, the central Arctic Ocean is perennially covered by sea ice, but considerable areas on the surrounding margins become ice-free during summers, which facilitate massive sediment entrainment in the processes of new ice formation or anchor ice release (e.g., Nürnberg et al., 1994; Darby et al., 2011). The sediment-laden ice is generally transported by wind driven circulation via the anticyclonic Beaufort Gyre in the Amerasian Basin and the Transpolar Drift over the Eurasian Basin, with the transit across the Arctic Ocean usually taking 3–4 years (**Figure 1**; Rigor, 1992).

While sea ice is believed to predominate sediment transportation and deposition in interglacial, modern-like environments (Polyak et al., 2010), iceberg rafting and other glacigenic processes played a major role during glacial intervals, when large, at least partially marine based ice sheets formed at the Arctic Ocean perimeter (**Figure 1**). However, the impact of glaciations on sedimentation in the Arctic Ocean was not straightforward, being controlled by a complex set of processes and paleogeographic settings. For example, the development of ice shelves in the central Arctic Ocean during glacial times, indicated by extensive seafloor data (Jakobsson et al., 2014, and references therein), may have strongly affected the surface circulation system and blocked sediment transportation in large areas, especially in the western Arctic (Polyak et al., 2009; Niessen et al., 2013; Jakobsson et al., 2016). Maximal sediments delivery to the central Arctic Ocean may have occurred during deglaciation intervals when circulation was not constrained by ice shelves, while the collapsing ice sheets provided massive inputs of icebergs and meltwater. Such events are marked in sedimentary records by peaks of coarse Ice Rafted Debris (IRD) traced to specific source regions, such as detrital carbonate layers indicative of North American (Laurentide) provenance (e.g., Clark et al., 1980; Bischof and Darby, 1997; Polyak et al., 2009; Stein et al., 2010). In addition, voluminous amounts of sediments were transported to the deep basins by glacial erosion on the

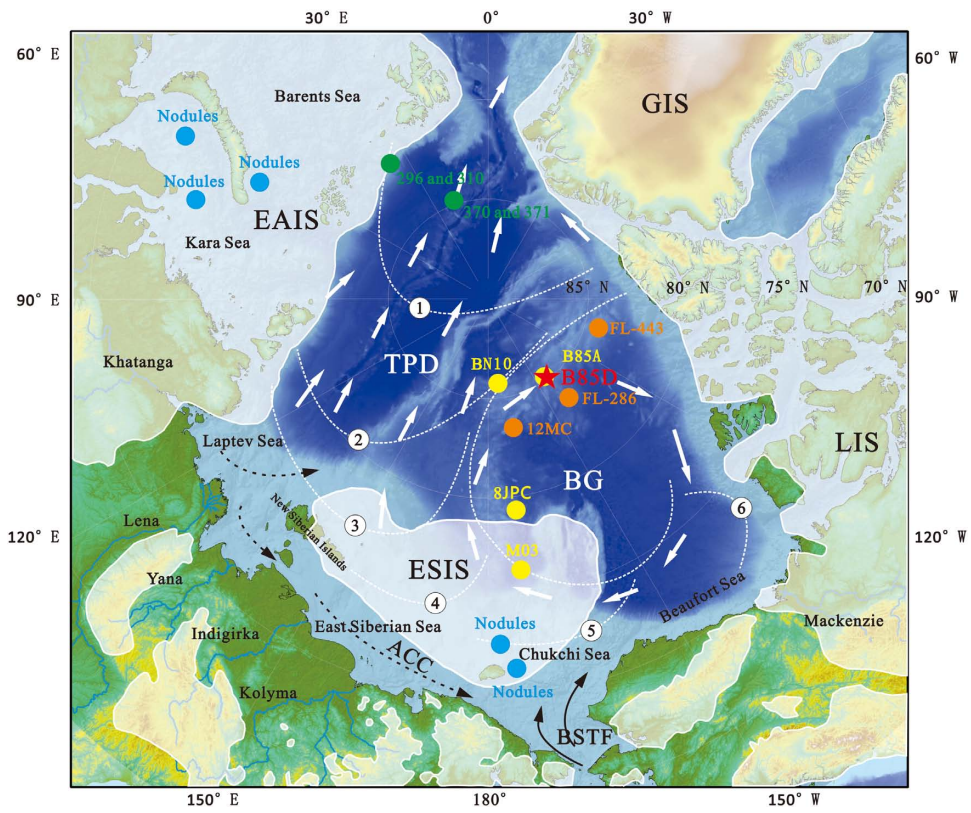

FIGURE 1 | Geographic setting of the study area and core locations. Core B85D (red star) is presented in this study; cores B85A, BN10, 8JPC and M03 (yellow circles) used for correlation are from Adler et al. (2009); Wang et al. (2013), and Wang et al. (2018), respectively. Orange and blue circles indicate Fe–Mn micro-nodule samples in the deep Arctic Ocean (Winter et al., 1997; Fagel et al., 2014) and Fe–Mn nodule samples on shelves (Baturin and Dubinchuk, 2011; Kolesnik and Kolesnik, 2015), respectively; green circles for water samples at 500 m depth from the Eurasian Basin (Westerlund and Öhman, 1992). Semi-transparent white areas show proposed maximal Pleistocene limits for Eurasian, Greenland, Laurentide, and East Siberia Ice Sheet (EAIS, GIS, LIS, and ESIS; Ehlers and Gibbard, 2007; Niessen et al., 2013). BG and TPD represent Beaufort Gyre and Trans Polar Drift, respectively; white dashed lines with numbers represent the number of years required for sea ice to reach the Fram Strait at present (Rigor, 1992); ACC and dashed lines with arrows represent Arctic coastal current; BSTF and black lines with arrows represent Bering Strait through flow Winsor and Chapman (2004).

shelves and downslope resedimentation, such as in debris flows (Niessen et al., 2013; Dove et al., 2014; Dong et al., 2017; O'Regan et al., 2017).

In addition to sea-ice and glacigenic sediment deposition, ocean currents may also play a significant role in sediment distribution across the Arctic Ocean. In particular, the Atlantic water running along the Arctic margins and submarine ridges at intermediate water depths may act as a sediment carrier by winnowing and redepositing fine-grained particles, possibly in combination with downslope brine movements into deep basins (Winkler et al., 2002; Dong et al., 2017; Dipre et al., 2018). However, the role of these processes in the overall Arctic Ocean sedimentation is not well understood. A periodic connection with the Pacific Ocean via the Bering Strait during high-sea-level intervals may also have a strong impact on sediment dynamics at the margins, especially in the western Arctic (e.g., Ortiz et al., 2009; Yurco et al., 2010; Yamamoto et al., 2017).

MATERIALS AND METHODS

Gravity sediment core ARC3-B85D (hereafter B85D) (147.080°W,85.140°N; water depth: 2060 m; **Figure 1**) was recovered from the Alpha Ridge, western Arctic Ocean, during the Third Chinese Arctic Expedition in 2008, along with a number of cores reported earlier (Wang et al., 2018), especially close to core B85A. This study focuses on the B85D sediments down to a depth of 1.3 m estimated to correspond to the upper and part of the middle Pleistocene, as discussed below. Lithostratigraphy of core B85D is typical for deep western Arctic Ocean sediments (e.g., Wang et al., 2018, and references therein) and shows no indication of turbidites. Besides samples from core B85D, 31 surface sediment samples collected during the Sixth Chinese Arctic Expedition in 2014 from the western Arctic and adjacent Bering Sea were analyzed to complement the existing major element and REE datasets across the Arctic shelves and deep basins (Nolting et al., 1996; Viscosi-Shirley et al., 2003; Astakhov et al., 2013).

The core was split along its axis, and XRF scanning was performed to obtain high-resolution Mn and Ca records at the Key Laboratory of Submarine Geosciences, State Oceanic Administration (SOA). Measurements were performed according to the approach suggested by Löwemark et al. (2011) with 2-mm downcore resolution and an exposure time of 5 s using the Mo-tube. After XRF scanning, the core was sampled in 1 cm increments and samples were dried at 40°C. A ground aliquot of 5 g was prepared for major element analysis by ICP-AES and REE analysis by ICP-MS at the State Key Laboratory of Marine Geology, Tongji University. Analytical precision was <5% for major and <8% for REE as checked with the national standard material of GSR-5, GSR-6 and GSR-9 after every 10 samples. For major elements (except partly evaporated Si) and REE in B85D samples, factor analysis was conducted using SPSS statistical software to evaluate the association of the REEs with different sedimentary phases. The Ce anomaly was calculated as $Ce/Ce^* = 2^*Ce/(La + Pr)$ (De Baar et al., 1983) to evaluate the enrichment of Ce relative to its neighbors La and Pr after the elements were normalized to the average compositions of the Post-Achean Australian Shale (PAAS) (Taylor and Mclennan, 1985).

Aliquots of the samples were washed over a 150 μm sieve. Residues were dried at 40°C and weighted after removing foraminifera for coarse grain content used as an estimate for IRD, although grains of other origins, such as Fe–Mn micronodules, may occur at some intervals. Planktic and benthic foraminifera species *Neogloboquadrina pachyderma* sinistral and *Cibicidoides wuellerstorfi* were counted, respectively. For accelerator mass spectrometry (AMS) ^{14}C dating, ∼7–10 mg of well-preserved specimens of *N. pachyderma* sinistral were picked from the >150 μm fraction in four samples at 0–1 cm, 3–4 cm, 6–7 cm, and 32–33 cm depth. AMS ^{14}C ages were determined at Beta Analytic Inc., Miami, FL, United States. The reported ^{14}C ages were used without a reservoir correction, which is poorly understood in the Arctic Ocean. While not very accurate, this approach provides a general age constraint for the youngest sediments. Lithostatigraphy coupled with the major element contents, IRD and foraminiferal abundances were used to constrain the age of B85D sediments by correlation to neighboring cores from the Alpha Ridge with a developed age model (Wang et al., 2018).

RESULTS

General Stratigraphy

Core B85D is characterized by sediment color cycles of interlaminating, generally brown and gray layers, representing cyclic changes in lithologic components and, thus, depositional environment (**Figure 2**). Four distinct groups of brown layers can be observed, at the depths of 0–4, 32–57, 65–95, and 103–119 cm. The upper boundaries of these layers are typically sharp, whereas the lower boundaries are disturbed by bioturbation, similar to cores reported elsewhere from the western Arctic Ocean (e.g., Polyak et al., 2004; Löwemark et al., 2012). Some thin sediment intervals display a distinct light yellowish to pinkish coloration, which allows us to identify them as the PW (pink-white) layers described in multiple studies from the western Arctic Ocean and attributed to glacigenic deposition of detrital carbonates from the Arctic Canada (Clark et al., 1980; Polyak et al., 2004; Stein et al., 2010; Cronin et al., 2013). The most prominent PW layers near the core top, at 46–52 cm, and at 96 cm were identified as PW3, PW2, and PW1, respectively (**Figure 2**).

The coarse grain (>150 μm) content in core B85D ranges from 0.5 to 14.7%, with the average of 4.4% (**Figure 2**). Above 78 cm depth, coarse fraction, consisting mostly of detrital grains, displays a close relationship to sediment color cycles, with generally high coarse grain content in gray layers and low in brown layers. The highest coarse grain content occurs at 32 cm depth at the top of a brown layer, showing a jump from less than 2% to almost 15%. Below 78 cm depth, coarse fraction is mostly composed of Fe–Mn micro-nodules. The main detrital ingredients of Fe–Mn micro-nodules are clay, quartz, feldspar and carbonate grains as well as foraminifera shells, which are coated and cemented by authigenic Fe–Mn (oxyhydr) oxide precipitates.

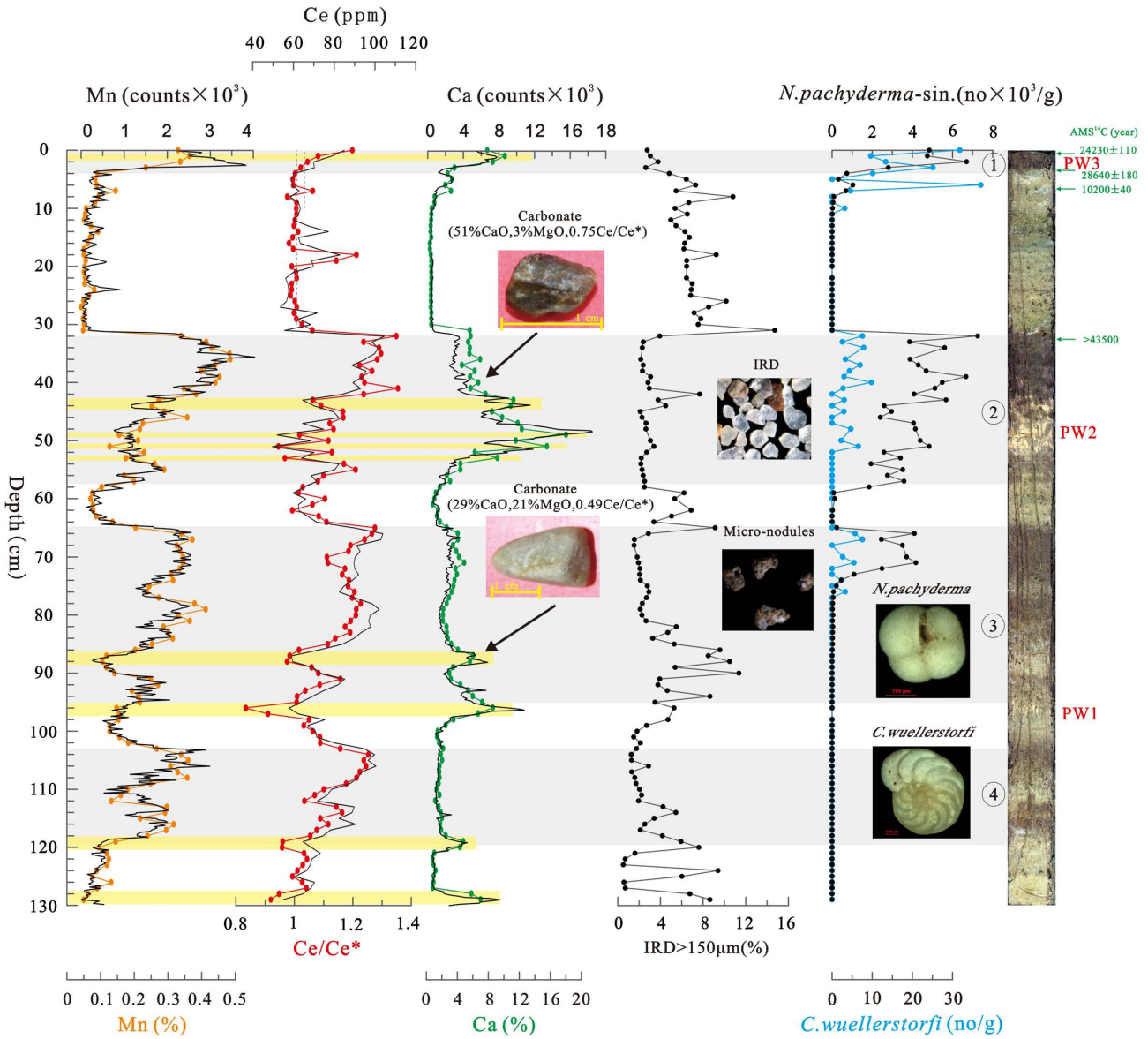

FIGURE 2 | General stratigraphy and sedimentary proxies investigated in core B85D, including Mn, Ca, and Ce XRF data, coarse grains (IRD) > 150 μm, and planktic and benthic foraminifera *N. pachyderma* (sin) and *C. wuellerstorfi*. Gray bars indicate groups of brown lithostratigraphic layers indicated by circle with number from group 1 to group 4; yellow bars indicate major Ca peaks; W3, PW2, and PW1 indicate pink-white layers. High-resolution Ca and Mn counts from XRF scanning are indicated by black lines; 2 cm-interval Ca and Mn content (%) from ICP-AES after total digestion by green and brown filled circles, respectively. Ce/Ce* represents Ce anomaly indicated by red filled circles. The photographs exemplify proxies investigated in the >150 μm fraction. Carbonate clasts next to the Ca curve are shown with their major element composition and Ce anomaly values.

Planktic foraminifera *N. pachyderma* sinistral and benthic *C. wuellerstorfi* are the dominant calcareous foraminifera > 150 μm. The depth distribution of these foraminifera is characterized by high abundances in the brown intervals of 0–12, 32–57, and 65–78 cm (**Figure 2**). The maximum abundance of *N. pachyderma* sinistral is up to 7250 no/g with an average of 2328 no/g in the brown layers. *C. wuellerstorfi* has generally lower abundances of 8 no/g average, with a maximum of 37 no/g. Above 78 cm depth, near-zero abundance of foraminifera is generally found in the gray layers, while sediments below this level contain practically no foraminifera at all.

Major Element Contents

Core Sediments

The Mn and Ca contents measured by different methods (XRF scanning and ICP-AES) display the same trends in the core depth profiles (**Figure 2**). Mn contents fluctuate along with the sediment color cycles, ranging from 0.04 to 0.5% with an average of ∼0.2% and the highest values found in the brown layers

(**Supplementary Table S1**). All gray layers have a baseline Mn content of ~0.05%. The most pronounced changes in Mn content plummeting from the highest to lowest values occur at the top of brown layers, while the increases in Mn at the bottom of brown layers are more gradual (**Figure 2**).

Total calcium content is characterized by a series of peaks occurring both in the groups of brown layers and in the gray layers, but are most common for transitional intervals (**Figure 2**). The highest peaks of Ca content are associated with coarse carbonate grains. Overall, variations in Ca content do not appear to be systematically related to Mn distribution (**Figure 2**).

Mn in Surface Sediments

Manganese contents in 31 surface sediment samples analyzed in this study are combined with published data as shown in **Figure 3**. Due to a large difference in sedimentation rates (e.g., Polyak et al., 2009; Stein et al., 2010), surface sediments analyzed may cover the time periods from 10s of years on the shelves to 1000s of years in the central Arctic Ocean, representing near-modern to average Holocene conditions, respectively. Early data on Mn content in surface sediment over the Arctic Ocean interior (Belov and Lapina, 1961), with more details added later for the Barents and Kara seas (Gurevich, 1995) and for the Laptev Sea (Nolting et al., 1996), provide a broad view of Mn geographic distribution (**Figure 3A**). This distribution indicates several important features: (1) the highest Mn contents (>0.5%) are confined to a prominent zone extending along the East Siberian margin and the Eurasian flank of the Lomonosov Ridge, closely following the mid-depth Atlantic water circulation; (2) low Mn contents (<0.2%) characterize large areas on the shelves and the central Amerasian Basin; (3) Mn distribution on the shelves is uneven and somewhat water depth-related; (4) no elevated Mn contents are found along the Gakkel Ridge, an active spreading zone.

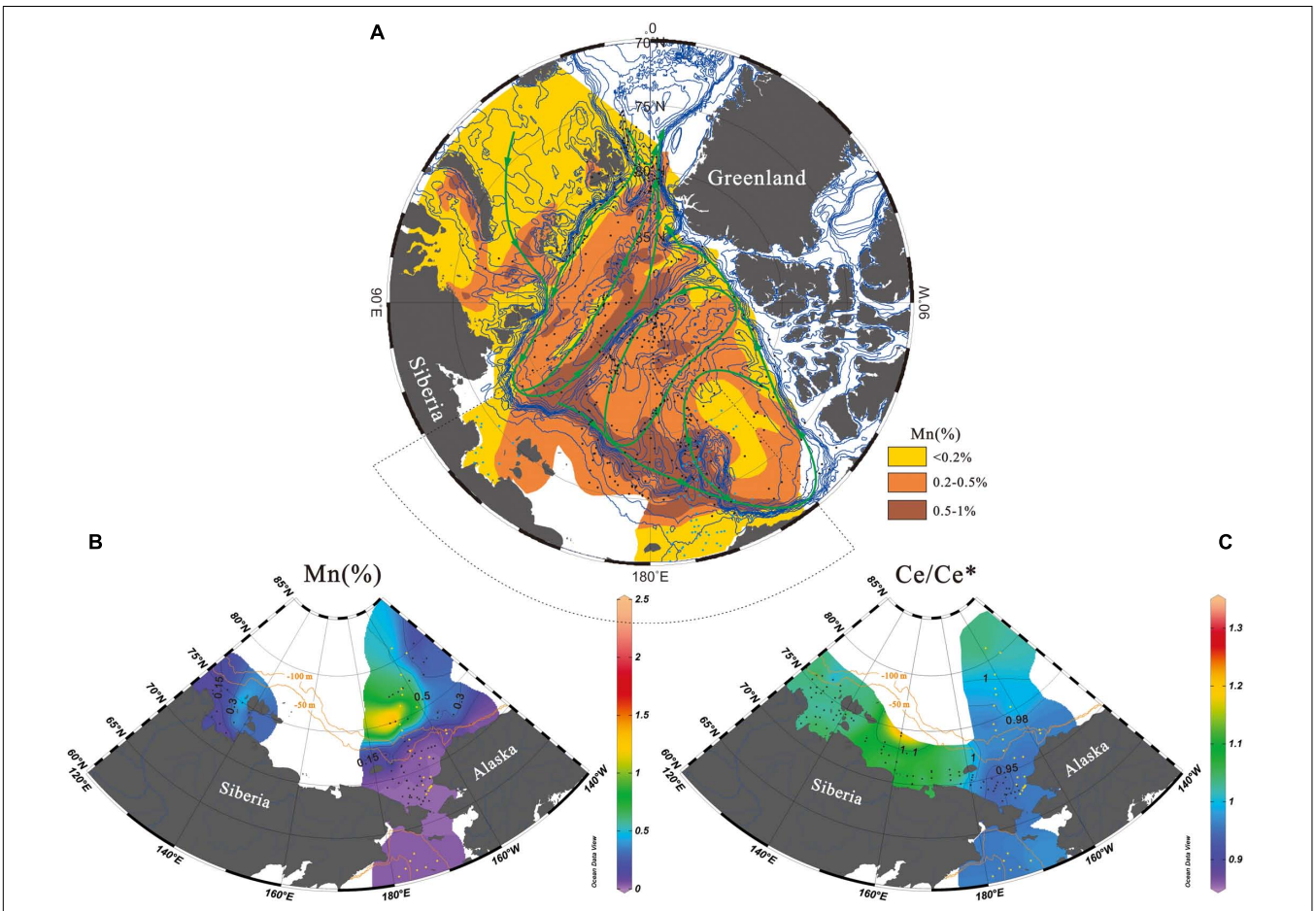

FIGURE 3 | Distribution of Mn and the Ce anomaly (Ce/Ce*) in surface sediments. **(A)** Generalized map of Mn distribution in the Arctic Ocean (from MnO data: Lapina and Belov, 1959; Belov and Lapina, 1961), Barents and Kara seas (from MnO data: Gurevich, 1995), and Siberian shelves (Nolting et al., 1996, and this study). Black and blue dots indicate data points for the central Arctic Ocean and Siberian margin, respectively. Numerous data points (not shown) were also used for the Barents-Kara shelves (Gurevich, 1995). Green arrows show mid-depth Atlantic water circulation (Rudels et al., 2004). Dotted box shows the location of inset for panels **(B,C)**. **(B)** Details of Mn distribution on the western Arctic shelves and adjacent basin. Yellow and black dots indicate data points from this study and from literature (Nolting et al., 1996; Astakhov et al., 2013), respectively. **(C)** Ce/Ce* distribution on the western Arctic shelves and adjacent basin. Yellow and black dots indicate data points from this study and from literature (Viscosi-Shirley et al., 2003; Astakhov et al., 2013), respectively. Ce anomaly calculated using La and Nd contents. Brown contours in **(B,C)** indicate 50 and 100 m isobaths.

More details on Mn distribution are featured along the East Siberian margin and adjacent shelves and deep basins (**Figure 3B**). Very low Mn contents of less than 0.15% were obtained on the shallow (<50–100 m) shelves of the Chukchi and Beaufort seas with the adjacent northern Bering Sea, as well as the inner Laptev Sea. High values of >0.5% mostly occur at intermediate depths off the shallow margin, such as the Chukchi Plateau, while the deep Canada Basin has distinctly lower values of <0.3%. In the Laptev Sea, Mn values somewhat increase toward the outer northeastern shelf away from the Lena River delta, while no data is available for the East Siberian Sea.

REE and Ce Anomaly Patterns

The total content of REE (ΣREE) in core B85D ranges from 122 to 218 ppm with an average of 172 ppm, just slightly lower than 185 ppm in PAAS (Taylor and Mclennan, 1985). Cerium makes up the largest part of the REE content with up to 49%, higher than 43% in PAAS. As shown in the factor analysis results (**Table 1**), two leading factors extracted from twenty four variables of the REE and major elements explain variances of 67.6 and 18.9%, respectively. Factor 1 closely relates the REE to Mn and Fe, and thus represents precipitation of the labile forms of these metals. Factor 2, in contrast, is defined by elements related to terrestrial inputs including two major rock types, carbonate-dominated and silicate-dominated.

Normalization of the REE values to chondritic composition indicates enrichment in light REE (LREE) and a strong depletion in Eu, typical for weathering of material similar in composition to the upper crust (Banner et al., 1988). In contrast, normalization to PAAS composition results in enrichments of Ce and middle REE (MREE). As shown in **Figure 4**, almost every sample displays the MREE enrichment independent of sediment lithology, while evident Ce enrichments characterize only Mn-rich brown layers.

TABLE 1 | Factor analysis results for REE and major elements in core B85D.

Factor 1	Loading	Histogram	Factor2	Loading	Histogram
(67.6%)		−1.0 0 1.0	**(18.9%)**		−1.0 0 1.0
Fe	0.686		Fe	0.662	
Mn	0.863		Ca	−0.868	
La	0.874		Al	0.878	
Ce	0.861		Ti	0.961	
Pr	0.888		Mg	−0.724	
Nd	0.902		P	0.757	
Sm	0.936		K	0.707	
Eu	0.913		Na	0.696	
Gd	0.978				
Tb	0.977				
Dy	0.973				
Ho	0.962				
Er	0.961				
Tm	0.947				
Yb	0.938				
Lu	0.933				

67.6% variances can be explained by factor1, 18.9% by factor 2; elements Mn and REE can be entirely constrained by factor1 with positive loading coefficients > 0.85, while element Fe was constrained by both factor1 and factor2; elements Ca and Mg hold negative loading with factor 2, different from elements Fe, Al, Ti, P, K, and Na.

Based on their Mn and Ca distribution, major sediment layers can be classified into four groups: Mn-rich brown layers; carbonate- and Mn-rich brown layers; gray layers; and carbonate-rich gray layers. Each group has a characteristic REE pattern (**Figure 4**). Both brown layer types are characterized by strong Ce enrichments with average Ce anomalies of 1.17 and 1.18, respectively, as opposed to gray layers where the Ce anomaly does not exceed 1.04. The most unusual geochemical pattern characterizes carbonate-rich gray layers which do not only have the lowest ΣREE, but also a negative average Ce anomaly of 0.96 that represents the depletion of Ce compared to PAAS.

The down core record of Ce anomaly in core B85D broadly matches the Mn content, with the highest Ce anomaly values (up to 1.35) occurring in brown layers (**Figure 2**). Wherever low values in Ce anomaly occur in either brown or gray layers (as low as 0.83), they generally coincide with peaks in Ca content (**Figure 2**). Cerium anomalies were also measured in carbonate gravels picked at 40 and 87 cm core depth, showing Ce anomaly values as low as 0.75 and 0.49, respectively (**Figure 2**). It is important to note that unlike Mn content, the Ce anomaly is determined by comparing the content of Ce to La and Pr in the same sample, so the Ce anomaly values in bulk sediment are sensitive to the REE pattern of any terrestrial or biogenic material that contributes significantly to the sediment volume, e.g., carbonate gravel with very low Ce anomalies. Sharp shifts in the Ce anomaly are also typical for the top of brown layers, especially at 32 and 65 cm depth, similar to drastic decreases in Mn content at these levels.

Cerium anomalies measured in the 31 surface sediment samples were combined with published data (**Figure 3C**). As the REE data reported by Viscosi-Shirley et al. (2003) lack Pr contents, the Ce anomaly was calculated using La and Nd, which introduces a small bias of ∼0.002 in comparison to the values generated in this study using La and Pr. Overall, the distribution of the Ce anomaly in surface sediments displays two obvious boundaries: between the Chukchi and East Siberia seas, and between the Chukchi Sea and the deep Amerasian Basin (**Figure 3C**). The latter boundary is mostly consistent with the Mn distribution, with the negative Ce anomaly values extending a bit further basinwards. The Ce anomaly boundary between the Chukchi and East Siberian shelves cannot be compared to the Mn distribution due to insufficient data. Positive Ce anomalies are prevalent over the East Siberian shelf extending into the Laptev Sea, with a maximum of 1.34, exceeding Ce anomaly values in the deep basin.

DISCUSSION

Stratigraphic Patterns of Mn Distribution

Stratigraphy of sedimentary proxies, including physical properties, foraminiferal abundance, sediment color, and Mn and Ca content, is widely used to evaluate the age of Arctic Ocean records on glacial-interglacial timescales (e.g.,

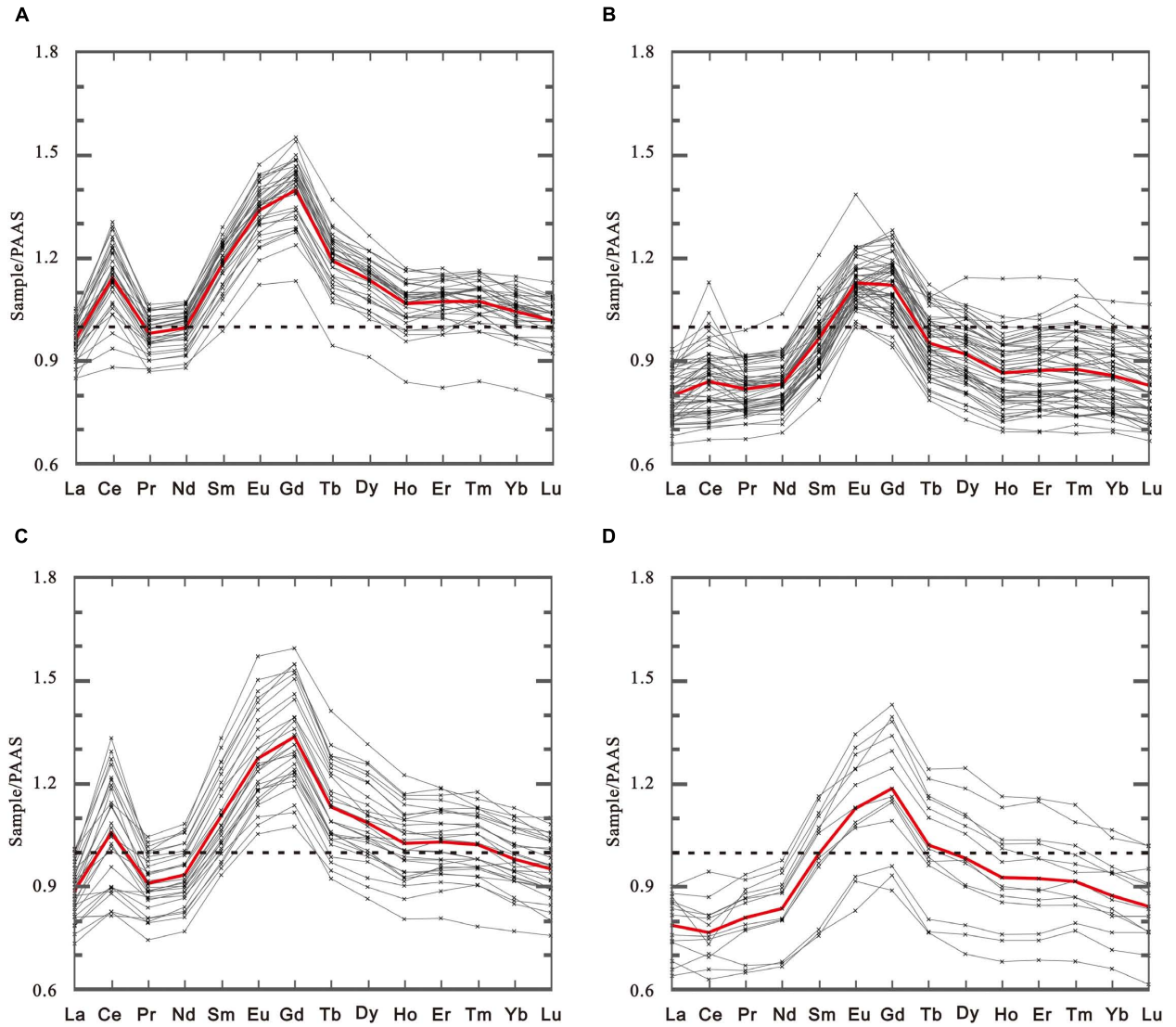

FIGURE 4 | Rare Earth Elements patterns in core B85D. Sediments are classified into four groups based on Mn (0.2%) and Ca (4.3%) contents: **(A)** Mn-rich brown layers with average Ce anomalies of 1.17, **(B)** Gray layers with average Ce anomalies of 1.04, **(C)** Carbonate- and Mn-rich brown layers with average Ce anomalies of 1.18, and **(D)** Carbonate-rich gray layers with average Ce anomalies of 0.96. All REE values are normalized to PAAS. Gray lines indicate patterns in individual samples; red lines indicate the averages in different groups; dashed lines indicate the ratio of 1 where the sample's REE content is equal to PAAS.

Jakobsson et al., 2000; O'Regan et al., 2008; Cronin et al., 2013; Schreck et al., 2018; Wang et al., 2018). The proxy distribution in core B85D (e.g., Mn and Ca contents: **Figure 5**) shares the same downcore pattern with a nearby core B85A that has been tuned to the orbital time scale based on its Mn record (Wang et al., 2018), which allows us to splice the B85A age model to core B85D with some adjustments. We note that the cyclostratigraphic approach used in Wang et al. (2018) and earlier studies (e.g., O'Regan et al., 2008; Adler et al., 2009; Cronin et al., 2013) yet needs to be verified by independent chronostratigraphic constraints.

The distribution of AMS^{14}C datings and Mn and Ca patterns suggests that the top of core B85D is comprised by MIS3 sediments (brown group 1) (**Figures 2**, **5**), while the younger stratigraphy is absent, possibly due to coring disturbance combined with very low sedimentation rates. The bottom of MIS3 was tentatively placed at the depth of a marked increase in foraminiferal abundance, preceding an increase in Mn (**Figure 5**). Identification of the broadly grouped interglacials MIS5, 7, and 9 is aligned with groups 2 to 4 of brown, Mn-rich layers (**Figure 2**), consistent with the B85A age model except for the placement of the bottom brown layer of group 3 into MIS8 (**Figure 5**). This adjustment is guided by the relation of a detrital carbonate layer PW1 to a glacial interval assigned by several authors to MIS8 (Stein et al., 2010; Dong et al., 2017). Global relative sea level pattern (e.g., Spratt and Lisiecki, 2016), also indicates an interval of anomalously high sea level within MIS8, probably corresponding to a pronounced interstadial.

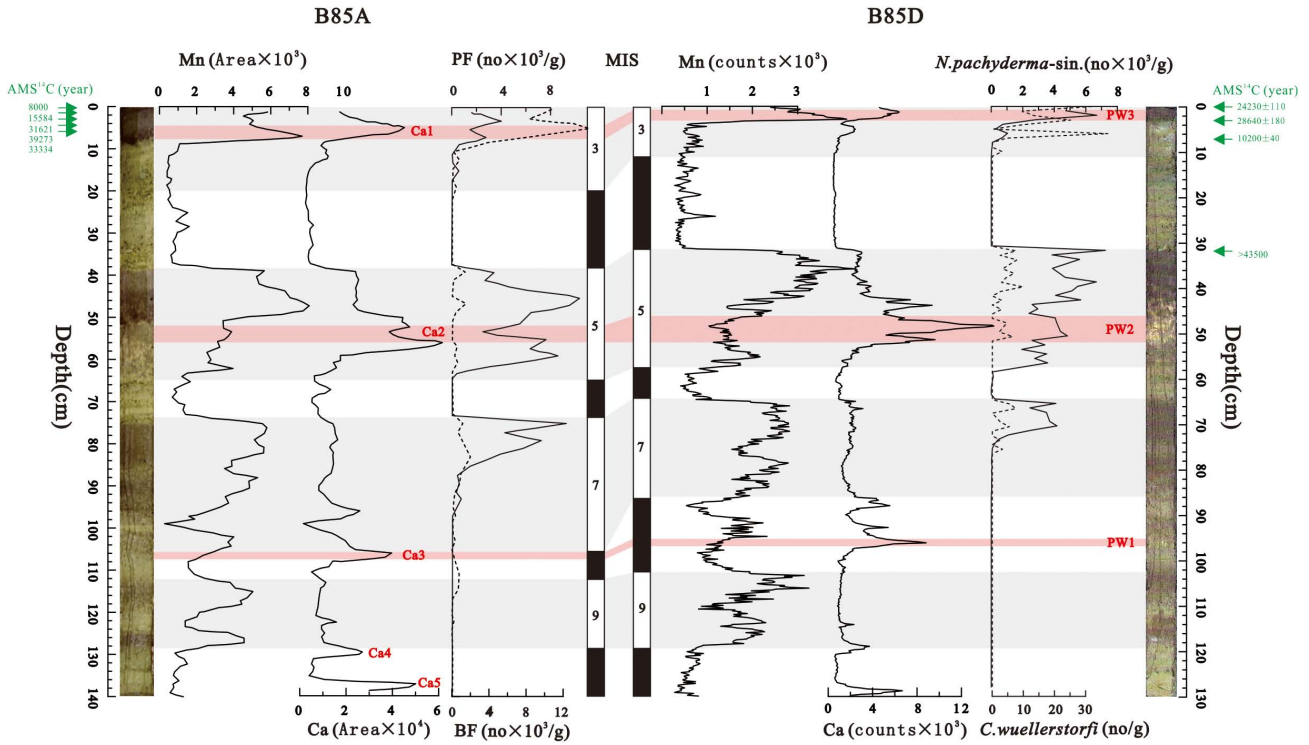

FIGURE 5 | Age model for core B85D facilitated by correlation to neighboring core B85A (Wang et al., 2018). Brown unit groups are highlighted by gray. Major Ca peaks are numbered Ca1 to Ca5. PF and BF indicate planktic and benthic foraminiferal abundances, respectively, in core B85A (Wang et al., 2018). Labels PW and pink bars indicate pink-white layers, with an estimated age of ∼110 ka for PW2 and ∼30–40 ka for PW3 (Polyak et al., 2009; Stein et al., 2010; Cronin et al., 2013). Green arrows with numbers indicate AMS^{14}C ages. Marine Isotope Stages (MIS) (Lisiecki and Raymo, 2005) are shown by white/black bars as estimated for B85A (Wang et al., 2018) and B85D (this study).

Overall, our age model, largely adopted from core B85A (Wang et al., 2018), implies that the 1.3 m-long sedimentary record of B85D reaches back to estimated MIS10, approximately 350 ka (**Figure 5**). Based on a linear interpolation between the assumed MIS boundaries, the average sedimentation rate is ∼0.4 cm/kyr, with the largest variability affecting glacial intervals, consistent with earlier estimates for the Alpha Ridge area (Polyak et al., 2009; Wang et al., 2018).

In order to resolve details of the regional stratigraphic Mn distribution better than in the strongly compressed B85D record, we compare it with other Arctic Ocean records characterized by higher sediment accumulation due to their location closer to the continental margin or at the foot of submarine ridges, as well as possibly lesser sea-ice coverage toward the fringes of the Beaufort Gyre (**Figure 1**) (Polyak et al., 2009; Stein et al., 2010; Schreck et al., 2018). An increase in average sedimentation rates up to an order of magnitude is apparent on a core transect from the Alpha Ridge to southern Mendeleev Ridge and the adjacent Chukchi Basin closer to the East Siberian margin (**Figure 6**).

As exemplified by core B85D, the strongest Mn enrichments in the stratigraphically compressed Alpha Ridge records appear to occur near the tops of interglacial/major interstadial intervals (**Figures 5**). Core BN10 located closer to the Transpolar Drift pathway at the distal end of the Mendeleev Ridge displays a Mn pattern similar to B85D, but with more discreet peaks, such as in the upper part of MIS5, when mean sea level fluctuated between −20 and −50 m (**Figure 6**) (Creveling et al., 2017). These peaks have been specifically defined as MIS5a and MIS5c in core 8JPC from the Mendeleev Ridge foot further south, where the stratigraphy shows yet more structure due to higher temporal resolution (Adler et al., 2009). The highest Mn peak in this record appears at MIS5c, seemingly contradicting the inference of increasing Mn contents toward the tops of interglacial intervals. However, if we consider higher sedimentation rates estimated for MIS5a in this core (7.5 cm/kyr vs. 1.8 cm/kyr for MIS 5c: Adler et al., 2009), the integral area of Mn curve versus age would still indicate higher fluxes during MIS 5a. Based on core M03 from the Chukchi Basin, the peak of Mn enrichment in MIS3 may also be inferred closer to the end of this interval (Wang et al., 2013). However, more investigation is needed for this interstadial that had sea level estimated as high as −40 m culminating around 40–50 ka (Pico et al., 2016).

Overall, we propose that the pattern of Mn distribution in compressed, sediment-starved records from the interior of the western Arctic Ocean exemplified by core B85D reflects a crude yet adequate pattern of Mn fluxes on glacial-interglacial time scales. While cores located closer to the continental margins provide more details, the actual Mn record may be distorted here by sediment dilution, especially during intervals of large glacigenic inputs (e.g., Schreck et al., 2018).

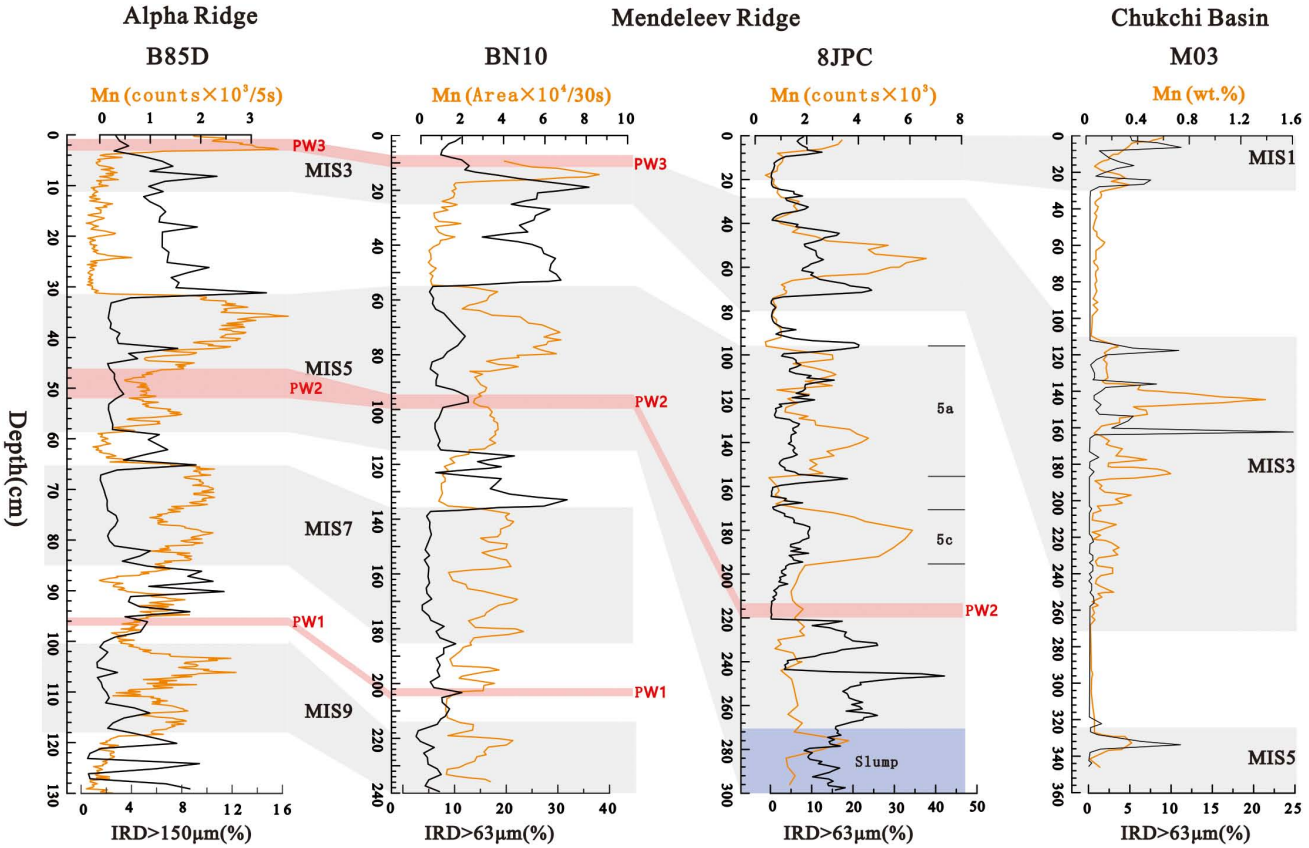

FIGURE 6 | Correlation of core B85D with earlier investigated records from the Alpha Ridge (BN10: Wang et al., 2018), Mendeleev Ridge (8JPC: Adler et al., 2009), and Chukchi Basin (M03: Wang et al., 2013). More structure is seen in the core stratigraphy with increase in sedimentation rates from the Alpha Ridge towards the Chukchi Basin. Pink bars with PW labels indicate pink-white detrital carbonate layers; gray bars labeled MIS1 to MIS9 indicate generalized interglacials and MIS3 interstadial; MIS5 substages 5a and 5c are also shown for core 8JPC. Note different core-depth scales.

Origin of Mn and Ce in Arctic Ocean Sediments

Both Mn and Ce are sensitive to ambient redox conditions, but respond somewhat differently to oxygen depletion in marine waters and sediments. Below the ocean mixed layer, Mn^{2+} is oxidized three times faster than Ce^{3+}, while in sediment pore waters Ce oxides are reduced prior to Mn oxides, and a combination of both processes determines the contents of both metals in the sediments (Moffett, 1990; Haley et al., 2004). Despite these differences in geochemical properties of Mn and Ce, as exemplified by core B85D, both metals express concurrent enrichments with a strong link to glacial-interglacial cyclicity, indicating common controls on their long-term deposition.

Most Mn in the Arctic Ocean (except for the Gakkel Ridge area) is delivered from rivers and coastal erosion (Guay and Falkner, 1997; Yunker et al., 2011; Macdonald and Gobeil, 2012). It has been suggested that Mn delivered in dissolved or suspended form is initially trapped on the extensive shelves (Macdonald and Gobeil, 2012), consistent with rather low Mn inputs in solution and suspended particulate material (SPM) coming directly from rivers (Rachold, 1999). Over time, Mn from riverine/coastal inputs will accumulate on the shelves. Due to relatively high primary production in these areas, sub- to anoxic conditions develop just below the sediment-water interface (Nolting et al., 1996; Gebhardt et al., 2005), leading to gradual dissolution of primary or diagenetic Mn species in sediments and re-precipitation of Mn (oxyhydr)oxides at the sediment-water interface, sometimes even with the diffusion of dissolved Mn into the bottom waters (e.g., Krauskopf, 1957; Sundby et al., 1986; Nolting et al., 1996; Laës et al., 2007; Middag et al., 2011). Transport of this re-precipitated Mn from the shelves ultimately leads to sedimentary Mn deposition in the Arctic Ocean interior. While sediments in the deep Arctic Ocean can also serve as Mn^{2+} sources due to early diagenetic remobilization, this process occurs in 10s of meters of these organic-poor sediments and thus should not have a considerable effect on Mn distribution in short records such as B85D (März et al., 2011a; Meinhardt et al., 2016).

In contrast to Mn, prior studies have not put a specific focus on the source and deposition of Ce in the central Arctic Ocean, just pointing out that REE are largely delivered by continental weathering (Johannesson and Zhou, 1999; Rachold, 1999). Data from core B85D indicate that Ce (among other REE) precipitates together with Mn and other redox-sensitive elements rather than being derived directly from terrestrial

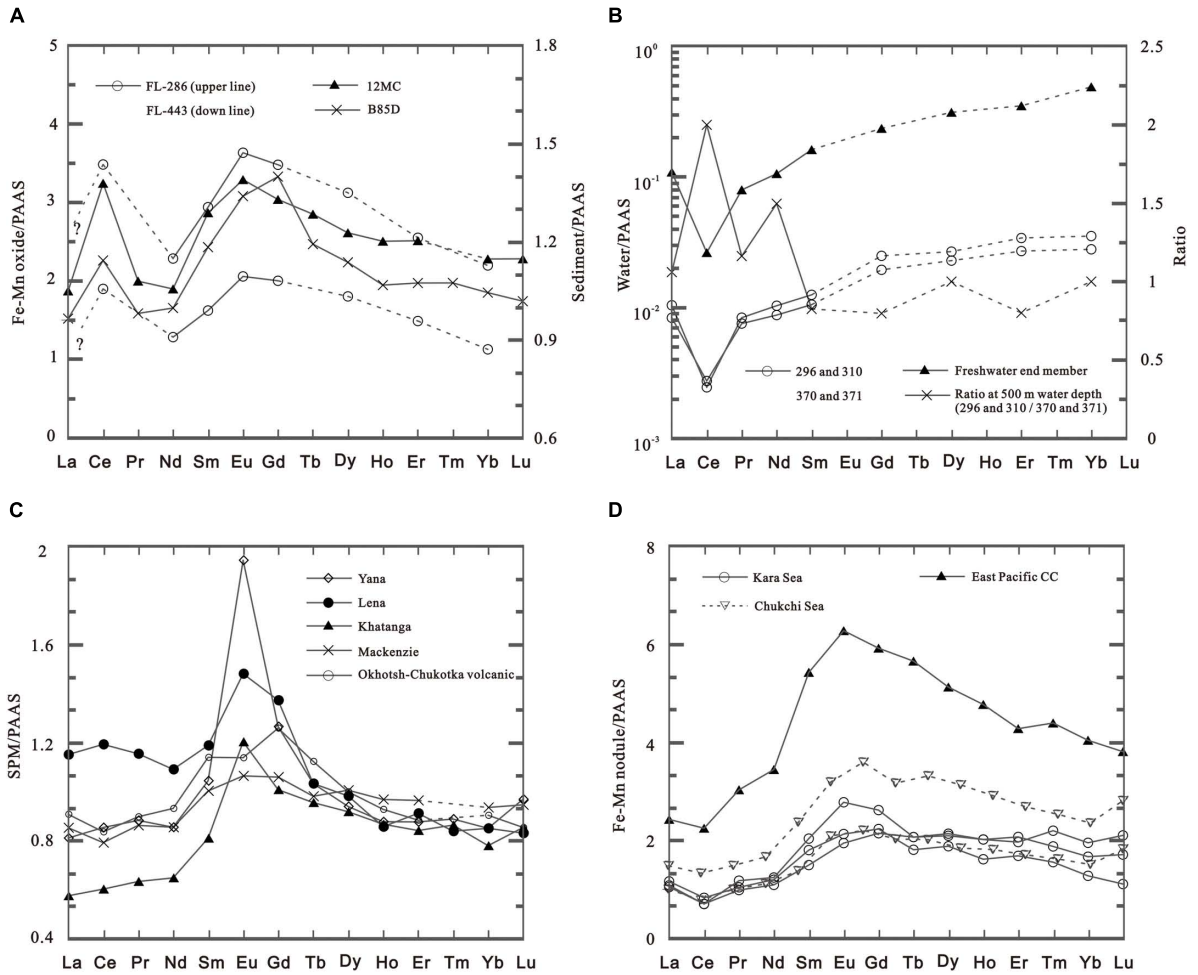

FIGURE 7 | Comparison of REE patterns between different sediment components: **(A)** Fe–Mn oxides leached from micro-nodules at the Alpha Ridge (FL-286 and FL443 from Winter et al., 1997, 12MC from Fagel et al., 2014), compared with that in the brown layer bulk sediments from B85D; **(B)** waters at 500 m depth in the Eurasian Basin (Westerlund and Öhman, 1992), with the REE ratio between two sites displayed to indicate lateral fractionation of Ce from the margins to the central Arctic Ocean; **(C)** suspended particle material in rivers and volcanic material (Fagel et al., 2014); **(D)** Fe–Mn nodules from the Kara Sea (Baturin and Dubinchuk, 2011), Chukchi Sea (Kolesnik and Kolesnik, 2015), and East Pacific Ocean (Jiang et al., 2009).

sources (**Table 1** and **Figure 2**). There has been a longstanding debate whether Mn (oxyhydr)oxides are carriers of REE, and specifically of Ce. Leaching experiments carried out on samples from Chesapeake Bay show that REE are not released when Mn (oxyhydr)oxides dissolve (Haley and Klinkhammer, 2002), while a similar study on sediments from the Fram Strait indicates that Mn (oxyhydr)oxides serve as important carriers for REE (Maccali et al., 2013). Although it has been demonstrated that Ce cannot be built into the crystal lattice of Mn (oxyhydr)oxides (Haley et al., 2004), our sedimentary data show that Ce record is associated with Mn and is strongly enriched in the Fe–Mn micro-nodules from the brown layers (**Figure 7A**), consistent with earlier results from the Alpha Ridge area (Winter et al., 1997). These patterns suggest that the behavior of Ce in the Arctic Ocean is not different from the rest of the world ocean in that dissolved Ce^{3+} tends to be oxidized in the water column (Westerlund and Öhman, 1992) and enriched in the sediments under oxic depositional conditions. The question is where sedimentary Ce in the Arctic Ocean comes from and how it is deposited and enriched in specific stratigraphic intervals.

In this study, we attempt to track the origin of Ce in the Arctic Ocean by comparing the Ce anomaly distribution in core B85D and in surface sediments from the potential source areas on the Siberian to Alaskan shelves. Dissolved REE inputs from rivers, lakes, and meltwater around the Arctic Ocean are characterized by negative Ce anomalies, becoming more negative toward the central Arctic Ocean as Ce^{3+} is being oxidized and precipitated out of the water column (**Figure 7B**; Westerlund and Öhman, 1992; Tepe and Bau, 2015). Cerium anomalies in riverine SPM range from negative values originating from the Mackenzie River and the Okhotsk-Chukotka volcanic belt to weakly positive anomalies from the East Siberian rivers (**Figure 7C**; Fagel et al., 2014). These patterns indicate that pronounced positive Ce anomalies in the central Arctic Ocean

sediments cannot originate from direct terrestrial inputs of Ce in solution or SPM without additional mechanisms for Ce^{3+} enrichment, such as by diagenesis on the shelf.

Reduction of Ce oxides in sediments and the following re-precipitation at the sediment-water interface may be indicated by positive Ce anomalies in surface sediments on the Siberian shelves (**Figure 3**). In contrast, strong negative Ce anomalies occur in Fe–Mn nodules from the shelves (**Figure 7D**). These nodules, widely distributed on the Arctic shelves, are partly covered with sediment, different from typical hydrogenous nodules with strong positive Ce anomalies but similar to diagenetic nodules with negative Ce anomalies (Baturin and Dubinchuk, 2011; Kolesnik and Kolesnik, 2015; Menendez et al., 2017). The link between the partial burial of Fe–Mn nodules into the sediment and their negative Ce anomalies is related to the differential diagenetic behavior of Mn and Ce. While Mn^{2+} released from buried sediments during diagenesis is re-oxidized at the sediment-water interface to form and grow Fe–Mn nodules, any released Ce^{3+} remains in solution for a longer time due to its slower redox kinetics, and can escape adsorption by or co-precipitation on the nodules. What this comparison of Ce anomalies in bulk surface sediments (**Figure 3**) and Fe–Mn nodules (**Figure 7D**) shows is that suboxic diagenetic processes lead to a remobilization of Mn and Ce, but slightly different redox kinetics can cause a certain degree of separation between them during re-precipitation under oxic conditions. The latter might explain why there is an overall agreement but no linear relationship between the Ce anomalies and Mn contents in surface sediments (**Figure 3**). This pattern also suggests that while both Ce and Mn distribution is related to early diagenetic processes, there are other factors that may determine their close relationship in paleo-records, such as in core B85D over the past 350 ka.

Regarding the re-distribution of Mn and Ce, the question remains on where the dissolved Ce^{3+} and Mn^{2+} were oxidized to ultimately generate the repeated enrichments in the central Arctic Ocean sediments. There is no evidence that diagenetically released, dissolved Mn^{2+} can overcome the redox barrier in the water column and be directly transported to the central Arctic Ocean without being oxidized and precipitated as Mn (oxyhydr)oxides, except for Mn^{2+} in the surface water delivered by rivers and sustained by photo-reduction (Middag et al., 2011). According to the distribution of Mn and Ce in recent to sub-recent surface sediments (**Figure 3**), geochemical conditions favorable for Ce and Mn precipitation widely exist on the continental margins under interglacial-type conditions. If the diagenetically released Ce^{3+} and Mn^{2+} were transported immediately after they diffused out of the shelf sediments, a deficiency of metal accumulations on the shelves would be expected in order to account for Mn and Ce enrichments in the central Arctic Ocean sediments. In contrast, Mn and Ce adsorption to fine-grained sediment particles or incorporation into Fe–Mn oxide micro-nodules provide a reasonable explanation for metal accumulations in the Arctic Ocean, consistent with the water column data (Tachikawa et al., 1997; Kondo et al., 2016). Overall, the reported patterns of Mn and Ce distribution in Arctic sediments are consistent with the notion that diagenetically released Ce^{3+} and Mn^{2+} are oxidized and precipitated at the sediment-water interface on the shelves before being transported to the central Arctic Ocean (Nolting et al., 1996; Gebhardt et al., 2005; Macdonald and Gobeil, 2012; Kondo et al., 2016).

Patterns of Mn and Ce Mobilization, Transport, and Deposition

Since the supply of oxidized Mn and related metals like Ce from the shelves controls its deposition in the deeper Arctic Ocean, sea level must be a critical factor in sedimentary Mn dynamics. During interglacials/major interstadials, relatively high sea levels keep large shelf areas under water, thus enabling diagenesis-induced remobilization of reactive metals and their export to the ocean interior. However, as discussed above, the strongest Mn and Ce enrichments in sediment records appear to occur not at the beginning or culmination of interglacial environments, when sea levels were rising and reaching the maxima, but toward the end of these intervals under falling sea levels (**Figure 8**). To resolve this counterintuitive relationship between sea level and the stratigraphic pattern, we need to consider not only the sources but also the transportation dynamics for Mn and related metals over glacial-interglacial cycles for evaluating the use of Mn cyclicity for orbital tuning.

It has been suggested that the major mechanism transporting sediments from the shelves to the central Arctic Ocean is related to sea ice (e.g., Nürnberg et al., 1994; Eicken et al., 2000; Darby, 2003; Darby et al., 2011), including export of Mn (oxyhydr)oxides (Holemann et al., 1999; Schoster, 2005). Recent data from Arctic sedimentary records also indicate a potentially considerable role of currents operating at different depth levels in the transportation of fine sediments (e.g., Dong et al., 2017; Dipre et al., 2018). These processes are likely to be strongly affected by changes in sea level. Broad and shallow Siberian shelves (Laptev, East Siberian, partly Chukchi and Kara seas) with prevailing water depths of <50–70 m are especially sensitive to sea-level fluctuations. Another hydrographic constraint is provided by the Bering Strait with a sill depth around 50 m, which to a large extent controls circulation and sea ice conditions on the Chukchi shelf and the adjacent western Arctic Ocean (e.g., Winsor and Chapman, 2004; Spall et al., 2018). Furthermore, Bering Strait opening/closing events have been suggested to affect not only circulation in the Arctic Ocean, but also in the North Atlantic, and thus the global climate on various time scales (Hu et al., 2015 and references therein). The Barents Sea, while overall considerably deeper than the Siberian shelves, can also be impacted by large sea level variations, which notably affect the distribution of Atlantic water branches between the Barents shelf and the Fram Strait (Schauer et al., 2002).

Distribution of Mn and Ce in surface sediments shows different patterns for the Chukchi Sea with the adjacent northern Bering Sea and Beaufort Sea, in comparison with the East Siberian and Laptev Sea shelves (**Figure 3**). On the Chukchi shelf and nearby areas with shallow water depths < 50–100 m affected by cross-shelf currents (Winsor and Chapman, 2004; Spall et al., 2018), Mn content is as low as <0.15%, that is within the range of the background lithogenic signature (Macdonald and Gobeil, 2012). This pattern indicates that a large portion of exchangeable

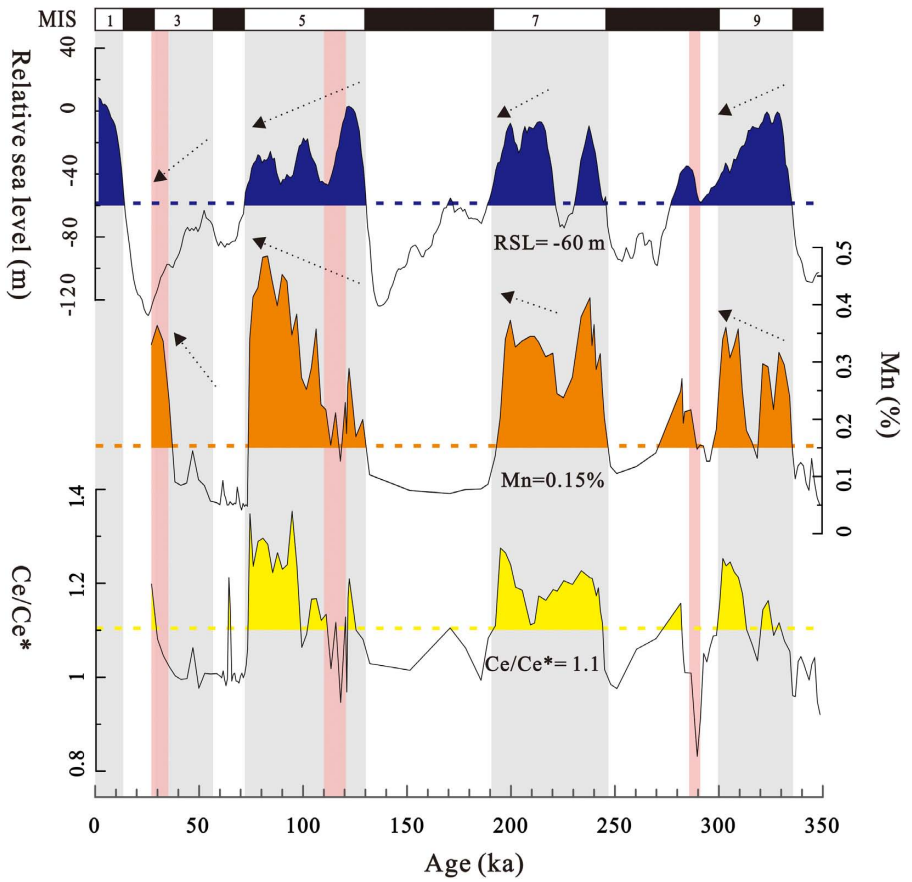

FIGURE 8 | Comparison of Mn and Ce/Ce* enrichment patterns in core B85D with global sea level changes over the last 350 ka (sea level data from Spratt and Lisiecki, 2016). Sea levels over –60 m below modern and corresponding Mn enrichments > 0.15% and Ce anomalies > 1.1 are shown in blue, red, and yellow, respectively. Corresponding time intervals (interglacials/major interstadials) are highlighted in gray. Pink bars indicate PW layers. Dashed arrows indicate the pattern of metal enrichments towards the end of generalized interglacial intervals and the corresponding decreasing trend in sea level.

Mn produced by diagenesis in these areas is being transported into the Arctic Ocean, consistent with Mn contents up to >1% in sediments on the outer Chukchi margin and adjacent borderland (**Figure 3**). SPM-mediated transportation of labile Mn off the Chukchi margin has been supported by direct observations on water column samples (Kondo et al., 2016). The location of these samples in the area of an especially strong cross-shelf circulation extending to the Canada Basin (Spall et al., 2018) provides a clear evidence of current transportation of exchangeable Mn into the interior Arctic Ocean. Similarly, Mn distribution in the Kara Sea indicates its removal from the shallow southern part of the shelf, except for the Yenisey River estuary area, and deposition in the deep troughs opening to the Arctic Ocean (Gurevich, 1995). In contrast, relatively high labile Mn contents occur on the outer Siberian shelves indicating the prevalence of its accumulation over export in these, mostly shallow areas with an extended sea-ice cover and generally low hydrodynamic activity (**Figure 3**; Gurevich, 1995; Nolting et al., 1996). Cerium anomaly on the western Arctic margins has a similar distribution, with low values characterizing the Chukchi Sea region and higher values on the adjacent borderland and on the Siberian shelves (**Figure 3**).

Overall, the geographic distribution of these exchangeable metals suggests that their main modern/recent sources to the western Arctic Ocean are the Chukchi, Beaufort and Bering seas with much less inputs from the Siberian shelves. This provenance does not appear to be consistent with the prevalent pattern of sea ice transportation. While practically all of the Arctic shelves can provide sea-ice transported sediments (Darby, 2003; Darby et al., 2011), the Laptev and East Siberian Seas are considered as major sources (e.g., Nürnberg et al., 1994; Eicken et al., 2000, 2005), with the role of the Chukchi and Beaufort shelves possibly increasing with the retreat of perennial ice in the warming climate (Eicken et al., 2005). In particular, the outer shelf area near the New Siberian Islands characterized with very high export of ice-entrained sediment (Eicken et al., 2000) has elevated Mn contents (**Figure 3**). On the other hand, the observed metal distribution is well consistent with the shelf circulation system with an overall sluggish circulation on the Siberian margin, whereas, Bering Sea originating currents impact the Chukchi and adjacent Beaufort shelves and propagate to the Canada Basin (Winsor and Chapman, 2004; Spall et al., 2018). The impact of currents on the seafloor is also demonstrated by sediment studies

indicating that coarser sediments occupy the shallow Chukchi shelf, whereas finer-grained deposits occur on the outer margin (Darby et al., 2009; Kolesnik and Kolesnik, 2015). In addition to cross-shelf currents, turbidity plumes caused by brine injections or sediment instabilities may transport sediments downslope (Haley and Polyak, 2013; Saint-Ange et al., 2014).

There is less up-to-date information available for the distribution of Mn in the interior of the Arctic Ocean. However, early data collected from the Soviet ice camps (Belov and Lapina, 1961) show a characteristic pattern with maximal Mn values occurring on the slopes of the Siberian margin and oceanic ridges along the pathway of mid-depth Atlantic-derived water (**Figure 3A**). Examination of the depth distribution of these sites shows that they are actually located at the lower edge or even slightly deeper than the core of the Atlantic water (∼200–900 m), consistent with the expected deposition of fine particles transported or resuspended by the current. Although sparse in the Arctic, reported velocity measurements of the slope boundary current along the Eurasian margin range between 1 and 5 cm/s (Coachman and Barnes, 1963), sufficient for transportation of fine particles in suspension. Modeled velocities for the ocean interior are lower than 1 cm/s (Zhang et al., 1998), but higher values have been measured over submarine ridges, consistent with the observed nepheloid layers (Hunkins et al., 1969). Recent sediment core and geophysical studies further indicate past current-controlled erosion/deposition regimes in the deep Arctic Ocean, such as north of the Chukchi margin (Hegewald and Jokat, 2013; Dipre et al., 2018), which implies a potentially strong effect of the mid-depth circulation on the exchangeable metal (re)distribution during those times.

Glacial-interglacial sea-level changes should have dramatically impacted Mn and Ce transportation and deposition. In the process of initial sea level lowering with the onset of glaciation, sediments that accumulated on the shelves during the interglacial can be flushed into the ocean, as shown for various continental margins (e.g., Milliman and Syvitski, 1992). This should have involved the metal-enriched deposits on the Siberian shelf formed due to a restricted removal during interglacial conditions as discussed above. The flushing of these deposits during sea-level fall can explain the stratigraphic pattern of Mn and Ce in the Arctic Ocean interior with peaks occurring near the top of interglacial/major interstadial intervals (**Figure 8**). Further sea level lowering should have terminated metal export from the shelves as the closing of the ∼50 m-deep Bering Strait shuts down circulation in the Chukchi Sea, while sea level fall below ∼50–70 m exposes nearly all of the Siberian shelves, thus precluding their hydrographic exchange with the Arctic Ocean.

There is practically no data on circulation conditions in the Arctic Ocean during low sea levels. It is reasonable to infer that resuspension on the outer shelf and formation of downslope turbidity plumes intensified, especially with the growth of ice sheets at the Arctic periphery. Circulation of the submerged Atlantic layer should be affected by the shallowing of the Barents Sea, which would reroute the Atlantic water flow through the Fram Strait, potentially leading to shallower circulation in the Arctic Ocean (e.g., Schauer et al., 2002). Further regression and ice-sheet growth could potentially minimize the Atlantic inflow, especially with the formation of extensive ice shelves and their grounding on submarine ridges, notably the trans-Arctic Lomonosov Ridge (Jakobsson et al., 2016). This, together with the lack of exchange with the shelves can account for a deficiency of Mn and related metals in glacial stratigraphic intervals in Arctic Ocean sediment cores.

It is intriguing that the depths of ∼50–70 m, critical for the Arctic shelf-ocean exchange, correspond to the highest gradients in global sea level glacial/interglacial variations (**Figure 8**), suggesting a potential role of the Arctic Ocean in this variability. Indeed, numerical simulations indicate the impact of the Bering Strait opening/closing on the circulation in the North Atlantic, and thus on the global climate (Hu et al., 2015). While this connection needs more investigation, the coherence of major transitions in the global sea level and in the Arctic Mn and Ce records may provide an important criterion for their synchronization. Nevertheless, the apparent non-linear relationship of the Mn and Ce contents with the sea level during interglacials indicates that the cyclostratigraphic approach to Mn records can be used only for generalized discrimination between glacial and interglacia/major interstadiall intervals. The same pattern may also complicate chronostratigraphic tuning of other proxies, such as microfossil abundances (Marzen et al., 2016), which closely co-vary with Mn in Artic Ocean sediments (Polyak et al., 2004, 2013; Cronin et al., 2013; Wang et al., 2018). More insights into the nature and dynamics of Mn enrichments are needed to comprehend their relationship with the global climatic and sea-level changes, which may aid a better tuning of Mn stratigraphic records.

SUMMARY AND CONCLUSION

The aim of this study was to gain a better understanding on the paleoceanographic significance of Mn in Quaternary Arctic Ocean sediments, where this labile metal forms consistent enrichment cycles as demonstrated by numerous studies (e.g., Jakobsson et al., 2000; Polyak et al., 2004; Stein et al., 2010; Wang et al., 2018). Distribution of Mn along with a concurrent occurrence of Ce, an REE metal that complements the Mn dynamics, was investigated in surface sediments from the Arctic Ocean and adjacent shelves as well as in sediment core ARC3-B85D from the Alpha Ridge. The sediment stratigraphy of this core was constrained by correlation to nearby cores with an earlier developed age model (Wang et al., 2018) resulting in an age span for B85D estimated as ∼350 kyr (Marine Isotope Stages 3–10). Despite a compressed nature of this 130 cm-long record, its major lithostratigraphic features on glacial-interglacial time scales are consistent with other sedimentary records throughout the western Arctic Ocean. Both Mn contents and Ce anomalies show a distinct stratigraphic pattern with overall low/high values in glacial/interglacial intervals, respectively, where the general co-variation of Ce with Mn was demonstrated for the first time. Within this stratigraphic variability, presumably corresponding to the global climatic and sea-level cycles, the peak values of both Mn and Ce appear to occur near the end of interglacial/major interstadial intervals.

The understanding of this paleoceanographic pattern is facilitated by analyzing the distribution of Mn and Ce, expressed as Ce anomaly (Ce/Ce*), in surface (modern/submodern) sediments from the continental shelves and the central Arctic Ocean, with most details captured for the Siberian margin. Multiple studies indicate that Mn imported from rivers and coastal deposits undergoes a diagenetic transformation on the Arctic shelves, but the dynamics of its further transportation and deposition, including cyclic enrichment in the interglacial sediments, were not well understood. Likewise, high positive Ce anomalies in the B85D record cannot be easily explained as under modern conditions Ce in the Arctic Ocean can form only negative to weakly positive anomalies. It has been suggested that Mn (oxyhydr)oxides are largely transported by sea ice formed over the shallow shelves (Holemann et al., 1999; Schoster, 2005). However, the pattern of Mn and Ce distributions in surface sediments also suggests a new interpretation highlighting the role of currents on labile metal transportation. This pattern notably features low concentrations of both Mn and Ce in the Chukchi Sea and on the adjacent shelves of the Bering and Beaufort seas, in contrast to considerably higher values along the outer Chukchi and East Siberian margin and adjacent oceanic ridges and plateaus. A similar picture is observed for Mn in the Kara Sea, with high concentrations in the deep troughs. This pattern is more consistent with the larger impact of hydrographic circulation rather than sea-ice transportation, especially in relation to the Bering Strait throughflow and resulting cross-shelf currents (e.g., Spall et al., 2018). The transport of labile metals by currents is now confirmed by direct observations in the Chukchi Sea (Kondo et al., 2016). Available data on further Mn distribution in the Arctic Ocean indicate highest values along the slopes of the continental margin and oceanic ridges, in an apparent agreement with the flow of the mid-depth circulation of Atlantic origin. We thus infer that transportation of Mn and related labile metals from the shelf and their eventual deposition in the Arctic Ocean is primarily mediated by cross-shelf and mid-depth oceanic currents, with potential contribution from other processes such as sea ice and downslope turbidity plumes. Further investigation of the modern and past mid-depth circulation is key for a more conclusive explanation of the exchangeable metal sedimentation in the Arctic Ocean.

The proposed transport and depositional system has to be radically affected by glacial-interglacial sea-level changes, especially with respect to the shallow Siberian shelves and the Bering Strait. Sea-level falls below ∼50–70 m depths should have entirely stopped both the Bering Strait throughflow and the hydrographic and sediment-dynamic interaction between most of the Siberian margin and the central Arctic Ocean. This sea-level impact can explain the cyclic glacial-interglacial distribution of Mn and Ce in the deep-sea Arctic sediment cores. We further attribute the increase of Mn and Ce values toward the top of interglacial/major interstadial intervals to flushing of the accumulated shelf sediments with their high labile metal contents by the falling sea level. This interpretation implies that a conventional cyclostratigraphic approach to sedimentary Mn enrichments can adequately approximate general glacial-interglacial cycles, but may not be used as a more accurate chronostratigraphic tool. Tuning of the Arctic Ocean Mn records to global climatic/sea-level variations might be improved by our comprehension of the Arctic labile metal geochemistry and related sediment dynamics in the stratigraphic perspective.

AUTHOR CONTRIBUTIONS

LY initiated this project and was in charge of data analysis, drawing, and writing. CM carried out the key job in geochemistry and editing. LP provided the basic data of modern Mn contents, and was in charge of the chronostratigraphy building, and has carried out a lot of the paleoenvironmental explanation and editing. XY and WZ were involved in experiment and data analysis.

FUNDING

This study was funded by the National Natural Science Foundation of China under contract no. 41106048, and was performed as part of the Chinese Special Project on Arctic Ocean Marine Geology Investigation under contract no. CHINARE 2012-2017-03-02 from the Chinese Arctic and Antarctic Administration. LP contribution was supported by the United States National Science Foundation award PLR-1404370.

ACKNOWLEDGMENTS

We thank the crew members and scientists onboard *RV Xuelong* for their support during the Third Chinese Arctic Expedition, and the Ministry of Finance of China for funding this research. We also thank Dr. Peijun Qiao for technical support with element analysis and two reviewers, who helped improving the manuscript.

SUPPLEMENTARY MATERIAL

The Supplementary Material for this article can be found online at: https://www.frontiersin.org/articles/10.3389/feart.2018.00236/full#supplementary-material

TABLE S1 | Major and rare earth elements contents in Core B85D sediments.

REFERENCES

Abbott, A. N., Haley, B. A., McManus, J., and Reimers, C. E. (2015). The sedimentary flux of dissolved rare earth elements to the ocean. *Geochim. Cosmochim. Acta* 154, 186–200. doi: 10.1016/j.gca.2015.01.010

Adler, R. E., Polyak, L., Ortiz, J. D., Kaufman, D. S., Channell, J. E., Xuan, C., et al. (2009). Sediment record from the western Arctic Ocean with an improved Late Quaternary age resolution: HOTRAX core HLY0503-8JPC, Mendeleev Ridge. *Glob. Planet. Change* 68, 18–29. doi: 10.1016/j.gloplacha.2009.03.026

Astakhov, A. S., Wang, R., Crane, K., Ivanov, M. V., and Gao, A. (2013). Lithochemical classification of the Arctic depositional environments (Chukchi Sea) by methods of multivariate statistic. *Geochem. Int.* 51, 303–325. doi: 10.1134/S001670291302002X

Banner, J. L., Hanson, G. N., and Meyers, W. J. (1988). Rare earth element and Nd isotopic variations in regionally extensive dolomites from the burlington-keokuk formation (Mississippian): implications for REE mobility during carbonate diagenesis. *J. Sediment. Res.* 58, 415–432. doi: 10.1306/212F8DAA-2B24-11D7-8648000102C1865D

Baturin, G. N., and Dubinchuk, V. T. (2011). The composition of ferromanganese nodules of the Chukchi and East Siberian seas. *Dokl. Earth Sci.* 440, 1258–1264. doi: 10.1134/S1028334X11090029

Bau, M., and Koschinsky, A. (2009). Oxidative scavenging of cerium on hydrous Fe oxide: evidence from the distribution of rare earth elements and yttrium between Fe oxides and Mn oxides in hydrogenetic ferromanganese crusts. *Geochem. J.* 43, 37–47. doi: 10.2343/geochemj.1.0005

Bau, M., Schmidt, K., Koschinsky, A., Hein, J., Kuhn, T., and Usui, A. (2014). Discriminating between different genetic types of marine ferro-manganese crusts and nodules based on rare earth elements and yttrium. *Chem. Geol.* 381, 1–9. doi: 10.1016/j.chemgeo.2014.05.004

Belov, N. A., and Lapina, N. N. (1961). *Donnye Otlozheniya Arkticheskogo Bassejna (Seafloor Sediments of the Arctic Basin)*. Leningrad: Morskoj Transport, 150.

Bischof, J. F., and Darby, D. A. (1997). Mid-to Late Pleistocene ice drift in the western Arctic Ocean: evidence for a different circulation in the past. *Science* 277, 74–78. doi: 10.1126/science.277.5322.74

Clark, D. L., Whitman, R. R., Morgan, K. A., and Mackey, S. D. (1980). *Stratigraphy and Glacial-Marine Sediments of the Amerasian Basin, Central Arctic Ocean*. Boulder, CO: Geological Society of America. doi: 10.1130/SPE181-p1

Coachman, L., and Barnes, C. (1963). The movement of Atlantic water in the Arctic Ocean. *Arctic* 16, 8–16. doi: 10.14430/arctic3517

Creveling, J. R., Mitrovica, J. X., Clark, P. U., Waelbroeck, C., and Pico, T. (2017). Predicted bounds on peak global mean sea level during marine isotope stages 5a and 5c. *Quat. Sci. Rev.* 163, 193–208. doi: 10.1016/j.quascirev.2017.03.003

Cronin, T. M., Polyak, L., Reed, D., Kandiano, E., and Marzen, R. E. (2013). A 600-ka Arctic sea-ice record from Mendeleev Ridge based on ostracodes. *Quat. Sci. Rev.* 79, 157–167. doi: 10.1016/j.quascirev.2012.12.010

Darby, D. (2003). Sources of sediment found in sea ice from the western Arctic Ocean, new insights into processes of entrainment and drift patterns. *J. Geophys. Res.* 108:3257. doi: 10.1029/2002JC001350

Darby, D., Ortiz, J., Polyak, L., Lund, S., Jakobsson, M., and Woodgate, R. (2009). The role of currents and sea ice in both slowly deposited central Arctic and rapidly deposited Chukchi–Alaskan margin sediments. *Glob. Planet. Change* 68, 58–72. doi: 10.1016/j.gloplacha.2009.02.007

Darby, D. A., Myers, W. B., Jakobsson, M., and Rigor, I. (2011). Modern dirty sea ice characteristics and sources: the role of anchor ice. *J. Geophys. Res. Oceans* 116:C09008. doi: 10.1029/2010JC006675

De Baar, H. J. W., Bacon, M. P., and Brewer, P. G. (1983). Rare-earth distributions with a positive Ce anomaly in the Western North Atlantic Ocean. *Nature* 301, 324–327. doi: 10.1038/301324a0

Dipre, G. R., Polyak, L., Kuznetsov, A. B., Oti, E. A., Ortiz, J. D., Brachfeld, S. A., et al. (2018). Plio-Pleistocene sedimentary record from the Northwind Ridge: new insights into paleoclimatic evolution of the western Arctic Ocean for the last 5 Ma. *Arktos* 4:24. doi: 10.1007/s41063-018-0054-y

Dong, L., Liu, Y., Shi, X., Polyak, L., Huang, Y., Fang, X., et al. (2017). Sedimentary record from the Canada Basin, Arctic Ocean: implications for late to middle Pleistocene glacial history. *Clim. Past* 13, 511–531. doi: 10.5194/cp-13-511-2017

Dove, D., Polyak, L., and Coakley, B. (2014). Widespread, multi-source glacial erosion on the Chukchi margin, Arctic Ocean. *Quat. Sci. Rev.* 92, 112–122. doi: 10.1016/j.quascirev.2013.07.016

Ehlers, J., and Gibbard, P. L. (2007). The extent and chronology of Cenozoic Global Glaciations. *Quat. Int.* 164–165, 6–20. doi: 10.1016/j.quaint.2006.10.008

Eicken, H., Gradinger, R., Gaylord, A., Mahoney, A., Rigor, I., and Melling, H. (2005). Sediment transport by sea ice in the Chukchi and Beaufort Seas: increasing importance due to changing ice conditions? *Deep Sea Res. Part II* 52, 3281–3302. doi: 10.1016/J.dsr2.2005.10.006

Eicken, H., Kolatschek, J., Freitag, J., Lindemann, F., Kassens, H., and Dmitrenko, I. (2000). A key source area and constraints an entrainment for basin-scale sediment transport by Arctic sea ice. *Geophys. Res. Lett.* 27, 1919–1922. doi: 10.1029/1999GL011132

Elderfield, H., Hawkesworth, C., Greaves, M., and Calvert, S. (1981). Rare earth element geochemistry of oceanic ferromanganese nodules and associated sediments. *Geochim. Cosmochim. Acta* 45, 513–528. doi: 10.1016/0016-7037(81)90184-8

Elderfield, H., and Sholkovitz, E. R. (1987). Rare earth elements in the pore waters of reducing nearshore sediments. *Earth Planet. Sci. Lett.* 82, 280–288. doi: 10.1016/0012-821X(87)90202-0

Fagel, N., Not, C., Gueibe, J., Mattielli, N., and Bazhenova, E. (2014). Late Quaternary evolution of sediment provenances in the Central Arctic Ocean: mineral assemblage, trace element composition and Nd and Pb isotope fingerprints of detrital fraction from the Northern Mendeleev Ridge. *Quat. Sci. Rev.* 92, 140–154. doi: 10.1016/j.quascirev.2013.12.011

Gebhardt, A. C., Schoster, F., Gaye-Haake, B., Beeskow, B., Rachold, V., Unger, D., et al. (2005). The turbidity maximum zone of the Yenisei River (Siberia) and its impact on organic and inorganic proxies. *Estuar. Coast. Shelf Sci.* 65, 61–73. doi: 10.1016/j.ecss.2005.05.007

Glasby, G. (1973). Mechanisms of enrichment of the rarer elements in marine manganese nodules. *Mar. Chem.* 1, 105–125. doi: 10.1016/0304-4203(73)90010-8

Guay, C. K. H., and Falkner, K. K. (1997). Barium as a tracer of Arctic halocline and river waters. *Deep Sea Res. Part II Top. Stud. Oceanogr.* 44, 1543–1569. doi: 10.1016/S0967-0645(97)00066-0

Gurevich, V. I. (1995). *Recent Sedimentogenesis and Environment on the Arctic Shelf of Western Eurasia*. Available at: https://brage.bibsys.no/xmlui/bitstream/handle/11250/173022/Meddelelser131.pdf?sequence=1

Haley, B. A., Frank, M., Hathorne, E., and Pisias, N. (2014). Biogeochemical implications from dissolved rare earth element and Nd isotope distributions in the Gulf of Alaska. *Geochim. Cosmochim. Acta* 126, 455–474. doi: 10.1016/j.gca.2013.11.012

Haley, B. A., and Klinkhammer, G. P. (2002). Development of a flow-through system for cleaning and dissolving foraminiferal tests. *Chem. Geol.* 185, 51–69. doi: 10.1016/S0009-2541(01)00399-0

Haley, B. A., Klinkhammer, G. P., and McManus, J. (2004). Rare earth elements in pore waters of marine sediments. *Geochim. Cosmochim. Acta* 68, 1265–1279. doi: 10.1016/j.gca.2003.09.012

Haley, B. A., and Polyak, L. (2013). Pre-modern Arctic Ocean circulation from surface sediment neodymium isotopes. *Geophys. Res. Lett.* 40, 893–897. doi: 10.1002/grl.50188

Hegewald, A., and Jokat, W. (2013). Tectonic and sedimentary structures in the northern Chukchi region, Arctic Ocean. *J. Geophys. Res. Solid Earth* 118, 3285–3296. doi: 10.1002/jgrb.50282

Holemann, J., Schirmacher, M., Kassens, H., and Prange, A. (1999). Geochemistry of surficial and ice-rafted sediments from the Laptev Sea (Siberia). *Estuar. Coast. Shelf Sci.* 49, 45–59. doi: 10.1006/ecss.1999.0485

Hu, A., Meehl, G. A., Han, W., Otto-Bliestner, B., Abe-Ouchi, A., and Rosenbloom, N. (2015). Effects of the Bering Strait closure on AMOC and global climate under different background climates. *Prog. Oceanogr.* 132, 174–196. doi: 10.1016/j.pocean.2014.02.004

Hunkins, K., Thorndike, E. M., and Mathieu, G. (1969). Nepheloid layers and bottom currents in the Arctic Ocean. *J. Geophys. Res.* 74, 6995–7008. doi: 10.1029/JC074i028p06995

Jakobsson, M., Andreassen, K., Bjarnadóttir, L. R., Dove, D., Dowdeswell, J. A., England, J. H., et al. (2014). Arctic Ocean glacial history. *Quat. Sci. Rev.* 92, 40–67. doi: 10.1016/j.quascirev.2013.07.033

Jakobsson, M., Lovlie, R., Alhanbali, H. S., Arnold, E., Backman, J., and Morth, M. (2000). Manganese and color cycles in Arctic Ocean sediments constrain Pleistocene chronology. *Geology* 28, 23–26. doi: 10.1130/0091-7613(2000)28<23:MACCIA>2.0.CO;2

Jakobsson, M., Nilsson, J., Anderson, L., Backman, J., Björk, G., Cronin, T. M., et al. (2016). Evidence for an ice shelf covering the central Arctic Ocean during the penultimate glaciation. *Nat. Commun.* 7:10365. doi: 10.1038/ncomms10365

Jiang, X., Wen, L., Lin, X., and Yao, D. (2009). Enrichment mechanism of rare earth element in marine diagenetic ferromanganese nodule (In Chinese with English Abstract). *Mar. Sci.* 33, 114–121.

Johannesson, K. H., Hawkins, D. L., and Cortés, A. (2006). Do Archean chemical sediments record ancient seawater rare earth element patterns? *Geochim. Cosmochim. Acta* 70, 871–890. doi: 10.1016/j.gca.2005.10.013

Johannesson, K. H., and Zhou, X. (1999). Origin of middle rare earth element enrichments in acid waters of a Canadian High Arctic lake. *Geochim. Cosmochim. Acta* 63, 153–165. doi: 10.1016/S0016-7037(98)00291-9

Katsev, S., Sundby, B., and Mucci, A. (2006). Modeling vertical excursions of the redox boundary in sediments: application to deep basins of the Arctic Ocean. *Limnol. Oceanogr.* 51, 1581–1593. doi: 10.4319/lo.2006.51.4.1581

Kolesnik, O. N., and Kolesnik, A. N. (2015). Rare earth elements in ferromanganese nodules of the Chukchi Sea. *Lithol. Miner. Resour.* 50, 181–191. doi: 10.1134/S0024490215030050

Kondo, Y., Obata, H., Hioki, N., Ooki, A., Nishino, S., Kikuchi, T., et al. (2016). Transport of trace metals (Mn, Fe, Ni, Zn and Cd) in the western Arctic Ocean (Chukchi Sea and Canada Basin) in late summer 2012. *Deep Sea Res. Part I Oceanogr. Res. Pap.* 116, 236–252. doi: 10.1016/j.dsr.2016.08.010

Krauskopf, K. B. (1957). Separation of manganese from iron in sedimentary processes. *Geochim. Cosmochim. Acta* 12, 61–84. doi: 10.1016/0016-7037(57)90018-2

Laës, A., Blain, S., Laan, P., Ussher, S. J., Achterberg, E. P., Trëguer, P., et al. (2007). Sources and transport of dissolved iron and manganese along the continental margin of the Bay of Biscay. *Biogeosciences* 4, 181–194. doi: 10.5194/bg-4-181-2007

Lapina, N. N., and Belov, N. A. (1959). "Usloviya obrazovaniya donnyh otlozhenij Severnogo Ledovitogo okeana (Sedimentary environments in the Arctic Ocean)," in *Technical Report, NIIGA, AANII (Research Institute for Arctic Geology; Arctic and Antarctic Research Institute)*, Leningrad.

Lisiecki, L. E., and Raymo, M. E. (2005). A Pliocene-Pleistocene stack of 57 globally distributed benthic δ^{18}O records. *Paleoceanography* 20, 1003–1019. doi: 10.1029/2004PA001071

Löwemark, L., Chen, H., Yang, T., Kylander, M. E., Yu, E. F., Hsu, Y. W., et al. (2011). Normalizing XRF-scanner data: a cautionary note on the interpretation of high-resolution records from organic-rich lakes. *J. Asian Earth Sci.* 40, 1250–1256. doi: 10.1016/j.jseaes.2010.06.002

Löwemark, L., Marz, C., Oregan, M., and Gyllencreutz, R. (2014). Arctic Ocean Mn-stratigraphy: genesis, synthesis and inter-basin correlation. *Quat. Sci. Rev.* 92, 97–111. doi: 10.1016/j.quascirev.2013.11.018

Löwemark, L., O'Regan, M., Hanebuth, T., and Jakobsson, M. (2012). Late Quaternary spatial and temporal variability in Arctic deep-sea bioturbation and its relation to Mn-cycles. *Paleogeogr. Paleoclimatol. Paleoecol.* 365–366, 192–208. doi: 10.1016/j.palaeo.2012.09.028

Maccali, J., Hillairemarcel, C., Carignan, J., and Reisberg, L. (2013). Geochemical signatures of sediments documenting Arctic sea-ice and water mass export through Fram Strait since the Last Glacial Maximum. *Quat. Sci. Rev.* 64, 136–151. doi: 10.1016/j.quascirev.2012.10.029

Macdonald, R. W., and Gobeil, C. (2012). Manganese sources and sinks in the Arctic Ocean with reference to periodic enrichments in basin sediments. *Aquat. Geochem.* 18, 565–591. doi: 10.1007/s10498-011-9149-9

März, C., Stratmann, A., Matthiessen, J., Meinhardt, A. K., Eckert, S., Schnetger, B., et al. (2011a). Manganese-rich brown layers in Arctic Ocean sediments: composition, formation mechanisms, and diagenetic overprint. *Geochim. Cosmochim. Acta* 75, 7668–7687. doi: 10.1016/j.gca.2011.09.046

März, C., Vogt, C., Schnetger, B., and Brumsack, H.-J. (2011b). Variable Eocene-Miocene sedimentation processes and bottom water redox conditions in the Central Arctic Ocean (IODP Expedition 302). *Earth Planet. Sci. Lett.* 310, 526–537. doi: 10.1016/j.epsl.2011.08.025

Marzen, R. E., DeNinno, L. H., and Cronin, T. M. (2016). Calcareous microfossil-based orbital cyclostratigraphy in the Arctic Ocean. *Quat. Sci. Rev.* 140, 109–121. doi: 10.1016/j.quascirev.2016.07.004

Meinhardt, A.-K., März, C., Schuth, S., Lettmann, K., Schnetger, B., Wolff, J.-O., et al. (2016). Diagenetic regimes in Arctic Ocean sediments: implications for sediment geochemistry and core correlation. *Geochim. Cosmochim. Acta* 188, 125–146. doi: 10.1016/j.gca.2016.05.032

Meinhardt, A. K., März, C., Stein, R., and Brumsack, H. J. (2014). Regional variations in sediment geochemistry on a transect across the Mendeleev Ridge (Arctic Ocean). *Chem. Geol.* 369, 1–11. doi: 10.1016/j.chemgeo.2014.01.011

Menendez, A., James, R., Roberts, S. J., Peel, K. E., and Connelly, D. P. (2017). Controls on the distribution of rare earth elements in deep-sea sediments in the North Atlantic Ocean. *Ore Geol. Rev.* 87, 100–113. doi: 10.1016/j.oregeorev.2016.09.036

Middag, R., de Baar, H. J. W., Laan, P., and Klunder, M. B. (2011). Fluvial and hydrothermal input of manganese into the Arctic Ocean. *Geochim. Cosmochim. Acta* 75, 2393–2408. doi: 10.1016/j.gca.2011.02.011

Milliman, J. D., and Syvitski, J. P. (1992). Geomorphic/tectonic control of sediment discharge to the ocean: the importance of small mountainous rivers. *J. Geol.* 100, 525–544. doi: 10.1086/629606

Moffett, J. W. (1990). Microbially mediated cerium oxidation in sea water. *Nature* 345, 421–423. doi: 10.1038/345421a0

Niessen, F., Hong, J. K., Hegewald, A., Matthiessen, J., Stein, R., Kim, H., et al. (2013). Repeated Pleistocene glaciation of the East Siberian continental margin. *Nat. Geosci.* 6, 842–846. doi: 10.1038/ngeo1904

Nolting, R. F., Van Dalen, M., and Helder, W. (1996). Distribution of trace and major elements in sediment and pore waters of the Lena Delta and Laptev Sea. *Mar. Chem.* 53, 285–299. doi: 10.1016/0304-4203(95)00095-X

Nürnberg, D., Wollenburg, I., Dethleff, D., Eicken, H., Kassens, H., Letzig, T., et al. (1994). Sediments in Arctic sea ice: implications for entrainment, transport and release. *Mar. Geol.* 119, 185–214. doi: 10.1016/0025-3227(94)90181-3

O'Regan, M., Backman, J., Barrientos, N., Cronin, T. M., Gemery, L., Kirchner, N., et al. (2017). The De Long Trough: a newly discovered glacial trough on the East Siberian continental margin. *Clim. Past* 13, 1269–1284. doi: 10.5194/cp-13-1269-2017

O'Regan, M., King, J., Backman, J., Jakobsson, M., Pälike, H., Moran, K., et al. (2008). Constraints on the Pleistocene chronology of sediments from the Lomonosov Ridge. *Paleoceanography* 23:A1S19. doi: 10.1029/2007PA001551

Ortiz, J. D., Polyak, L., Grebmeier, J. M., Darby, D., Eberl, D. D., Naidu, S., et al. (2009). Provenance of Holocene sediment on the Chukchi-Alaskan margin based on combined diffuse spectral reflectance and quantitative X-Ray Diffraction analysis. *Glob. Planet. Change* 68, 73–84. doi: 10.1016/j.gloplacha.2009.03.020

Pico, T., Mitrovica, J. X., Ferrier, K. L., and Braun, J. (2016). Global ice volume during MIS 3 inferred from a sea-level analysis of sedimentary core records in the Yellow River Delta. *Quat. Sci. Rev.* 152, 72–79. doi: 10.1016/j.quascirev.2016.09.012

Polyak, L., Alley, R. B., Andrews, J. T., Brigham-Grette, J., Cronin, T. M., Darby, D. A., et al. (2010). History of sea ice in the Arctic. *Quat. Sci. Rev.* 29, 1757–1778. doi: 10.1016/j.quascirev.2010.02.010

Polyak, L., Best, K. M., Crawford, K. A., Council, E. A., and St-Onge, G. (2013). Quaternary history of sea ice in the western Arctic Ocean based on foraminifera. *Quat. Sci. Rev.* 79, 145–156. doi: 10.1016/j.quascirev.2012.12.018

Polyak, L., Bischof, J. F., Ortiz, J. D., Darby, D. A., Channell, J. E. T., Xuan, C., et al. (2009). Late Quaternary stratigraphy and sedimentation patterns in the western Arctic Ocean. *Glob. Planet. Change* 68, 5–17. doi: 10.1016/j.gloplacha.2009.03.014

Polyak, L., Curry, W. B., Darby, D. A., Bischof, J. F., and Cronin, T. M. (2004). Contrasting glacial/interglacial regimes in the western Arctic Ocean as exemplified by a sedimentary record from the Mendeleev Ridge. *Palaeogeogr. Palaeoclimatol. Palaeoecol.* 203, 73–93. doi: 10.1016/S0031-0182(03)00661-8

Rachold, V. (1999). "Major, trace and rare earth element geochemistry of suspended particulate material of east Siberian rivers draining to the Arctic Ocean," in *Land-Ocean Systems in the Siberian Arctic: Dynamics and History*, eds H. Kassens, H. A. Bauch, I. A. Dmitrenko, H. Eicken, H.-W. Hubberten, M. Melles, et al. (Berlin: Springer), 199–222. doi: 10.1007/978-3-642-60134-7_20

Rigor, I. (1992). Arctic Ocean buoy program. *ARCOS Newsl.* 44, 1–3.

Rudels, B., Jones, E. P., Schauer, U., and Eriksson, P. (2004). Atlantic sources of the Arctic Ocean surface and halocline waters. *Polar Res.* 23, 181–208. doi: 10.1111/j.1751-8369.2004.tb00007.x

Saint-Ange, F., Kuus, P., Blasco, S., Piper, D. J., Clarke, J. H., and MacKillop, K. (2014). Multiple failure styles related to shallow gas and fluid venting, upper slope Canadian Beaufort Sea, northern Canada. *Mar. Geol.* 355, 136–149. doi: 10.1016/j.margeo.2014.05.014

Sangiorgi, F., Brumsack, H., Willard, D. A., Schouten, S., Stickley, C. E., Oregan, M., et al. (2008). A 26 million year gap in the central Arctic record at the greenhouse-icehouse transition: looking for clues. *Paleoceanography* 23:A1S04. doi: 10.1029/2007PA001477

Schauer, U., Rudels, B., Jones, E., Anderson, L., Muench, R., Björk, G., et al. (2002). Confluence and redistribution of Atlantic water in the Nansen, Amundsen and Makarov basins. *Ann. Geophys.* 20, 257–273. doi: 10.5194/angeo-20-257-2002

Schoster, F. (2005). Terrigenous sediment supply and paleoenvironment in the Arctic Ocean during the late Quaternary: reconstructions from major and trace elements. *Rep. Polar Mar. Res.* 498:149.

Schreck, M., Nam, S.-I., Polyak, L., Vogt, C., Kong, G.-S., Stein, R., et al. (2018). Improved Pleistocene sediment stratigraphy and paleoenvironmental implications for the western Arctic Ocean off the East Siberian and Chukchi margins. *Arktos* 4:21. doi: 10.1007/s41063-018-0057-8

Soyol-Erdene, T.-O., and Huh, Y. (2013). Rare earth element cycling in the pore waters of the Bering Sea Slope (IODP Exp. 323). *Chem. Geol.* 358, 75–89. doi: 10.1016/j.chemgeo.2013.08.047

Spall, M., Pickart, R., Li, M., Itoh, M., Lin, P., Kikuchi, T., et al. (2018). Transport of Pacific water into the Canada Basin and the formation of the Chukchi Slope Current. *J. Geophys. Res. Oceans* 123, 7453–7471. doi: 10.1029/2018JC013825

Spielhagen, R. F., Baumann, K.-H., Erlenkeuser, H., Nowaczyk, N. R., Nørgaard-Pedersen, N., Vogt, C., et al. (2004). Arctic Ocean deep-sea record of northern Eurasian ice sheet history. *Quat. Sci. Rev.* 23, 1455–1483. doi: 10.1016/j.quascirev.2003.12.015

Spratt, R. M., and Lisiecki, L. E. (2016). A Late Pleistocene sea level stack. *Clim. Past* 12, 1079–1092. doi: 10.5194/cp-12-1079-2016

Stein, R., Matthiessen, J., Niessen, F., Krylov, A., Nam, S., and Bazhenova, E. (2010). Towards a better (litho-) stratigraphy and reconstruction of Quaternary paleoenvironment in the Amerasian Basin (Arctic Ocean). *Polarforschung* 79, 97–121. doi: 10.2312/polarforschung.79.2.97

Sundby, B., Anderson, L. G., Hall, P. O., Iverfeldt, Å, van der Loeff, M. M. R., and Westerlund, S. F. (1986). The effect of oxygen on release and uptake of cobalt, manganese, iron and phosphate at the sediment-water interface. *Geochim. Cosmochim. Acta* 50, 1281–1288. doi: 10.1016/0016-7037(86)90411-4

Sundby, B., Lecroart, P., Anschutz, P., Katsev, S., and Mucci, A. (2015). When deep diagenesis in Arctic Ocean sediments compromises manganese-based geochronology. *Mar. Geol.* 366, 62–68. doi: 10.1016/j.margeo.2015.04.005

Tachikawa, K., Handel, C., and Dupré, B. (1997). Distribution of rare earth elements and neodymium isotopes in settling particulate material of the tropical Atlantic Ocean (EUMELI site). *Deep Sea Res. Part I Oceanogr. Res. Pap.* 44, 1769–1792. doi: 10.1016/S0967-0637(98)00089-2

Taylor, S. R., and Mclennan, S. M. (1985). *The Continental Crust: Its Composition and Evolution. United States*. Boston, MA: Blackwell Scientific Publications, 1–328.

Tepe, N., and Bau, M. (2015). Distribution of rare earth elements and other high field strength elements in glacial meltwaters and sediments from the western Greenland Ice Sheet: evidence for different sources of particles and nanoparticles. *Chem. Geol.* 412, 59–68. doi: 10.1016/j.chemgeo.2015.07.026

Viscosi-Shirley, C., Mammone, K., Pisias, N. G., and Dymond, J. (2003). Clay mineralogy and multi-element chemistry of surface sediments on the Siberian-Arctic shelf: implications for sediment provenance and grain size sorting. *Cont. Shelf Res.* 23, 1175–1200. doi: 10.1016/S0278-4343(03)00091-8

Wang, R., Polyak, L., Xiao, W., Wu, L., Zhang, T., Sun, Y., et al. (2018). Late-Middle Quaternary lithostratigraphy and sedimentation patterns on the Alpha Ridge, central Arctic Ocean: implications for Arctic climate variability on orbital time scales. *Quat. Sci. Rev.* 181, 93–108. doi: 10.1016/j.quascirev.2017.12.006

Wang, R., Xiao, W., März, C., and Li, Q. (2013). Late Quaternary paleoenvironmental changes revealed by multi-proxy records from the Chukchi Abyssal Plain, western Arctic Ocean. *Glob. Planet. Change* 108, 100–118. doi: 10.1016/j.gloplacha.2013.05.017

Westerlund, S., and Öhman, P. (1992). Rare earth elements in the Arctic Ocean. *Deep Sea Res. A Oceanogr. Res. Pap.* 39, 1613–1626. doi: 10.1016/0198-0149(92)90051-T

Winkler, A., Wolf-Welling, T., Stattegger, K., and Thiede, J. (2002). Clay mineral sedimentation in high northern latitude deep-sea basins since the Middle Miocene (ODP Leg 151, NAAG). *Int. J. Earth Sci.* 91, 133–148. doi: 10.1007/s005310100199

Winsor, P., and Chapman, D. C. (2004). Pathways of Pacific water across the Chukchi Sea: a numerical model study. *J. Geophys. Res.* 109:C03002. doi: 10.1029/2003JC001962

Winter, B. L., Johnson, C. M., and Clark, D. L. (1997). Geochemical constraints on the formation of Late Cenozoic ferromanganese micronodules from the central Arctic Ocean. *Mar. Geol.* 138, 149–169. doi: 10.1016/S0025-3227(97)00013-3

Yamamoto, M., Nam, S.-I., Polyak, L., Kobayashi, D., Suzuki, K., Irino, T., et al. (2017). Holocene dynamics in the Bering Strait inflow to the Arctic and the Beaufort Gyre circulation based on sedimentary records from the Chukchi Sea. *Clim. Past* 13, 1111–1127. doi: 10.5194/cp-13-1111-2017

Yunker, M. B., Macdonald, R. W., Snowdon, L. R., and Fowler, B. R. (2011). Alkane and PAH biomarkers as tracers of terrigenous organic carbon in Arctic Ocean sediments. *Org. Geochem.* 42, 1109–1146. doi: 10.1016/j.orggeochem.2011.06.007

Yurco, L. N., Ortiz, J. D., Polyak, L., Darby, D. A., and Crawford, K. A. (2010). Clay mineral cycles identified by diffuse spectral reflectance in Quaternary sediments from the Northwind Ridge: implications for glacial–interglacial sedimentation patterns in the Arctic Ocean. *Polar Res.* 29, 176–197. doi: 10.1111/j.1751-8369.2010.00160.x

Zhang, J., Rothrock, D. A., and Steele, M. (1998). Warming of the Arctic Ocean by a strengthened Atlantic inflow: model results. *Geophys. Res. Lett.* 25, 1745–1748. doi: 10.1029/98GL01299

Conflict of Interest Statement: The authors declare that the research was conducted in the absence of any commercial or financial relationships that could be construed as a potential conflict of interest.